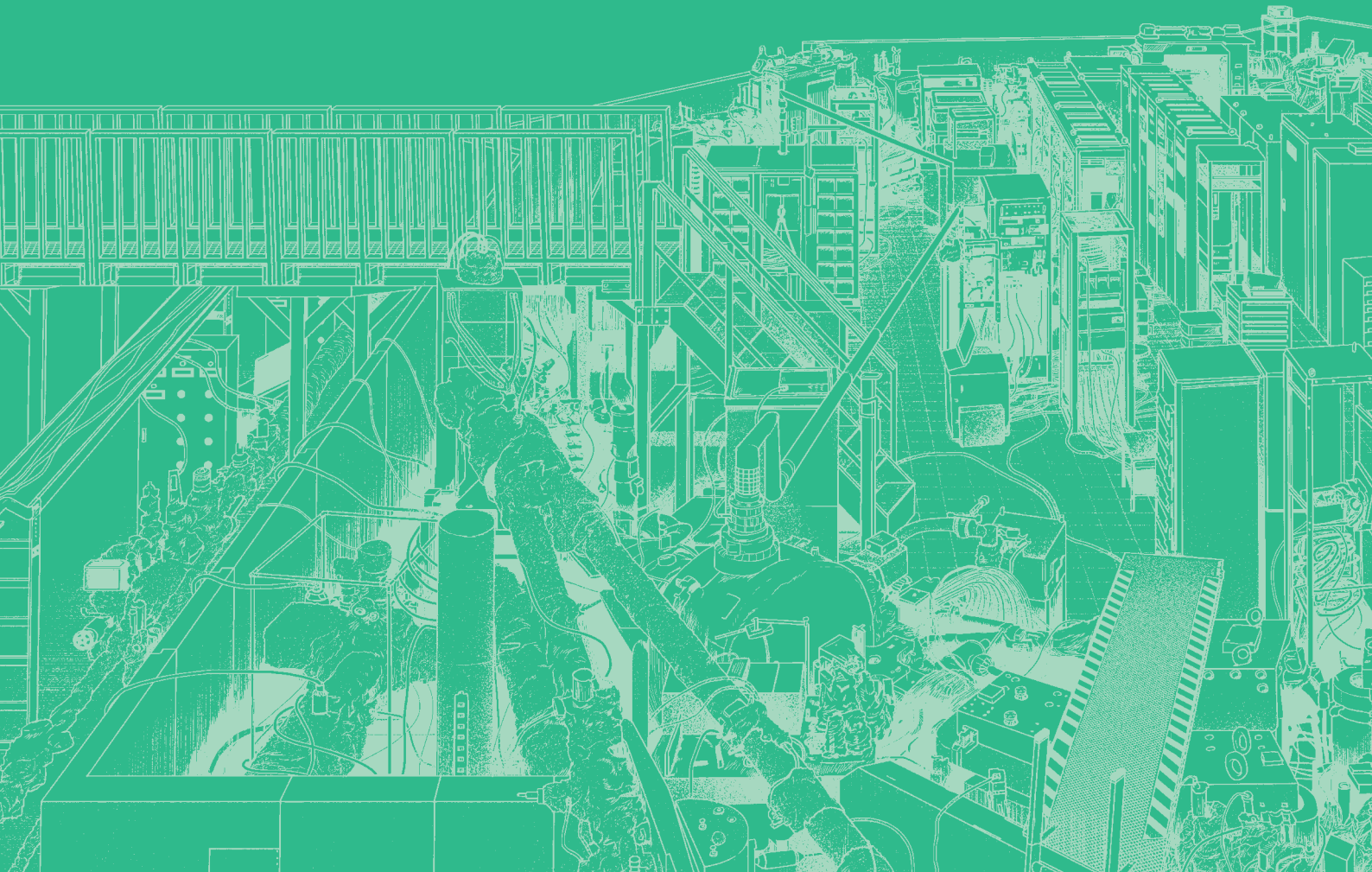


# Current Status of Light Sources and Beamlines





## Light Source in 2023

Yoshitaka Taira

UVSOR Synchrotron Facility, Institute for Molecular Science, Okazaki 444-8585, Japan

In FY2023, UVSOR-III was operated for users as scheduled for 36 weeks from end of May 2023 to March 2024. Monthly statistics of operation time and integrated beam current are shown in Fig. 1. From the beginning of April to early May, during which periodic inspections were conducted. The two weeks following the shutdown were allocated to the adjustment of the accelerator and beamlines.

The weekly operation schedule is as follows. Mondays are assigned to machine studies from 9:00 AM to 9:00 PM. User operation is assigned Tuesday through Friday, with Tuesday and Wednesday operating from 9:00 AM to 9:00 PM, and Thursday from 9:00 AM to 9:00 PM on Friday for 36 continuous hours. Thus, the user's beam time per week is 60 hours.

Instantaneous voltage drops due to lightning strikes occurred frequently during the July-August period. This caused beam dumps, leading to loss of operation time. Several insulation breakdowns of the high-voltage charging cable of the pulse power supply for the synchrotron first kicker have occurred, but have been restored by replacing the cable. A malfunction of the S-band pulse amplifier for the linear accelerator occurred, but has been addressed by adjusting the amplifier gain. We are considering updating the S-band pulse amplifier due to concerns that the problem may recur.

Injection efficiency of the electron beam into the storage ring started to decrease around January 2023. The injection efficiency is calculated as the ratio of the increase in the stored current value,  $\delta I$ , to the current value passing through the transport line between the booster synchrotron and the storage ring. Under normal conditions, the injection efficiency was 60~70% and  $\delta I$  was 0.4~0.6 mA/shot, but after January 2023, the efficiency dropped to 20~30% and  $\delta I$  0.1~0.3 mA/shot. The limited number of electrons that can be injected into the storage ring per week makes it difficult to continue 300 mA operation. Therefore, user operation has been conducted with the stored current value reduced to 200 mA since May 2023. Various investigations are continuing to determine the cause, but so far no clear cause has been identified. However, it has been confirmed that the quality of the electron beam extracted by the booster synchrotron has deteriorated. The vacuum ducts in the bending magnet section of the booster synchrotron have experienced multiple vacuum leaks, and there is concern that opening the ducts to the atmosphere may induce serious vacuum leaks, so it is currently impossible to visually check inside the ducts. All vacuum ducts in the bending magnet section are scheduled to be replaced with new

ones in the spring of 2025. At that time, we will check the inside of the vacuum ducts of the booster synchrotron to see if there are any foreign objects that are scattering the beam.

We started a design study for the future plan of UVSOR-IV. As a first step, we have analyzed the present magnetic lattice, seeking a possibility to reduce the emittance more [1]. Although, we did not find a solution to drastically reduce emittance, we have found a few interesting solutions that achieved lower emittance than the current situation. As the second step, we have started designing a totally new storage ring, which is close to the diffraction limit in the VUV range [2].

The light source development and utilization beamline BL1U, constructed under the support of Quantum Beam Technology Program by MEXT/JST, continue to develop new light source technologies and their applications such as free electron laser, coherent harmonic generation, coherent synchrotron radiation, coherent control [3], laser Compton scattered gamma rays [4, 5], and optical vortices [6].

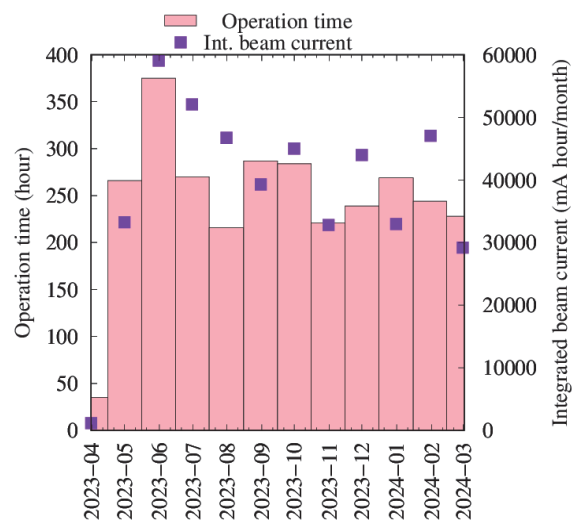


Fig. 1. Monthly statistics in FY2023.

- [1] E. Salehi and M. Katoh, Proceedings of IPAC2021 (2021) 3970.
- [2] E Salehi *et al.*, J. Phys.: Conf. Ser. **2420** (2023) 012062.
- [3] Y. Hikoska *et al.*, Sci. Rep. **13** (2023) 10292.
- [4] Y. Taira *et al.*, Phys. Rev. A **107** (2023) 063503.
- [5] H. Ohgaki *et al.*, Phys. Rev. Acc. Beams **26** (2023) 093402.
- [6] S. Wada *et al.*, Sci. Rep. **13** (2023) 22962.

# UVSOR Accelerator Complex

II

## Injection Linear Accelerator

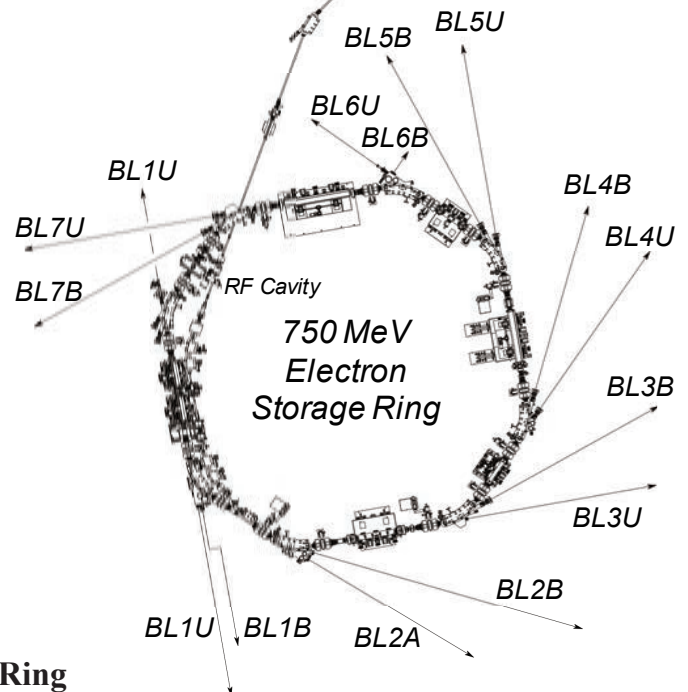
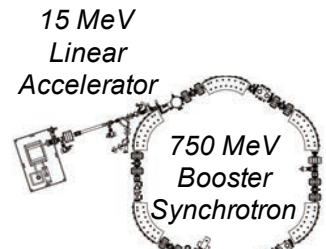
|                       |                         |
|-----------------------|-------------------------|
| Energy                | 15 MeV                  |
| Length                | 2.5 m                   |
| RF Frequency          | 2856 MHz                |
| Accelerating RF Field | $2\pi/3$ Traveling Wave |
| Klystron Power        | 1.8 MW                  |
| Energy Spread         | $\sim 1.6$ MeV          |
| Repetition Rate       | 1 Hz (Max. 3 Hz)        |

## Booster Synchrotron

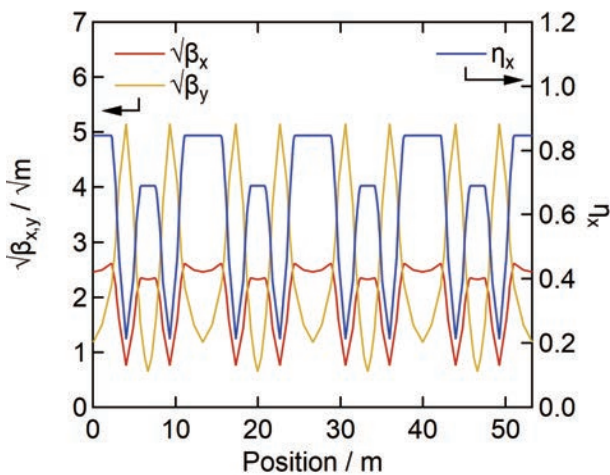
|                  |                         |
|------------------|-------------------------|
| Energy           | 750 MeV                 |
| Injection Energy | 15 MeV                  |
| Beam Current     | 15 mA (uniform filling) |
| Circumference    | 26.6 m                  |
| RF Frequency     | 90.1 MHz                |
| Harmonic Number  | 8                       |
| Bending Radius   | 1.8 m                   |
| Lattice          | FODO $\times 6$         |
| Betatron Tune    |                         |
| Horizontal       | 2.25                    |
| Vertical         | 1.25                    |
| Momentum         | 0.138                   |
| Compaction       |                         |
| Repetition Rate  | 1 Hz (Max. 3 Hz)        |

## UVSOR-III Storage Ring

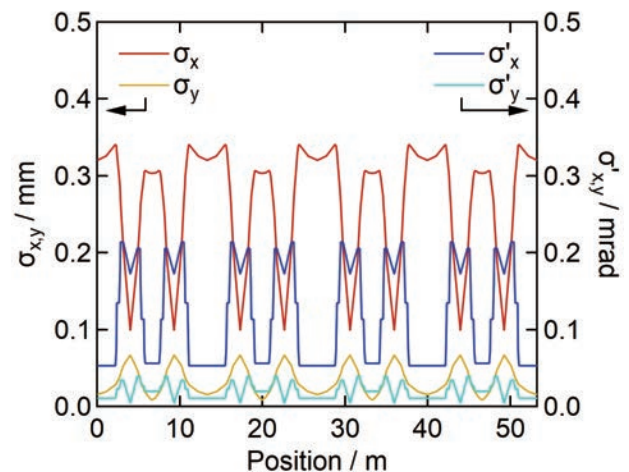
|                      |                                     |
|----------------------|-------------------------------------|
| Energy               | 750 MeV                             |
| Injection Energy     | 750 MeV                             |
| Normal Operation     | 300 mA (multi bunch)                |
| Current (Top-up)     | 40 mA (single bunch)                |
| Natural Emittance    | 17.5 nm rad                         |
| Circumference        | 53.2 m                              |
| RF Frequency         | 90.1 MHz                            |
| RF Voltage           | 120 kV                              |
| Harmonic Number      | 16                                  |
| Bending Radius       | 2.2 m                               |
| Lattice              | Extended DB $\times 4$              |
| Straight Section     | (4 m $\times$ 4)+(1.5 m $\times$ 4) |
| Betatron Tune        |                                     |
| Horizontal           | 3.75                                |
| Vertical             | 3.20                                |
| Momentum Compaction  | 0.030                               |
| Natural Chromaticity |                                     |
| Horizontal           | -8.1                                |
| Vertical             | -7.3                                |
| Energy Spread        | $5.26 \times 10^{-4}$               |
| Coupling Ratio       | 1%                                  |
| Natural Bunch Length | 128 ps                              |



## Electron Beam Optics of UVSOR-III Storage Ring



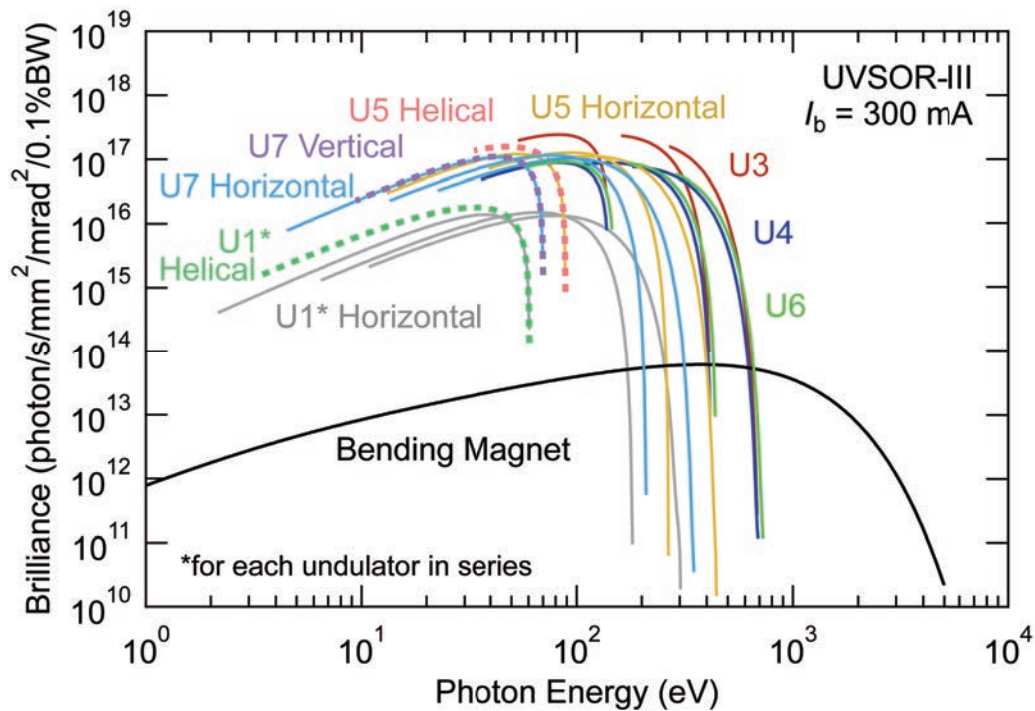
Horizontal / vertical betatron functions and dispersion functions



Horizontal / vertical electron beam size and beam divergences



## Insertion Devices



**Brilliance of radiation from the insertion devices (U1, U3, U4, U5, U6 and U7) and a bending magnet of UVSOR-III**

| <b>U1 Apple-II Undulator / Optical Klystron</b> |   |
|---|---|
| Number of Periods                               | 10 + 10   |
| Period Length                                   | 88 mm   |
| Pole Length                                     | 0.968 m + 0.968 m   |
| Pole Gap  | 24–200 mm   |
| Deflection Parameter                            | 7.36 (Max. Horizontal)<br>4.93 (Max. Vertical)<br>4.06 (Max. Helical) |

| <b>U5 Apple-II Variable Polarization Undulator</b> |  |
|--|--|
| Number of Periods                                  | 38   |
| Period Length                                      | 60 mm  |
| Pole Length  | 2.28 m   |
| Pole Gap   | 24–190 mm  |
| Deflection Parameter                               | 3.4 (Max. Horizontal)<br>2.1 (Max. Vertical)<br>1.8 (Max. Helical) |

| <b>U3 In-Vacuum Undulator</b> |            |
|-------------------------------|------------|
| Number of Periods             | 50         |
| Period Length                 | 38 mm      |
| Pole Length                   | 1.9 m      |
| Pole Gap                      | 16.5–40 mm |
| Deflection Parameter          | 1.8–0.24   |

| <b>U6 In-Vacuum Undulator</b> |           |
|-------------------------------|-----------|
| Number of Periods             | 26        |
| Period Length                 | 36 mm     |
| Pole Length                   | 0.94 m    |
| Pole Gap                      | 13–40 mm  |
| Deflection Parameter          | 1.78–0.19 |

| <b>U4 In-Vacuum Undulator</b> |          |
|-------------------------------|----------|
| Number of Periods             | 26       |
| Period Length                 | 38 mm    |
| Pole Length                   | 0.99 m   |
| Pole Gap                      | 13–40 mm |
| Deflection Parameter          | 2.4–0.19 |

| <b>U7 Apple-II Variable Polarization Undulator</b> |  |
|--|--|
| Number of Periods                                  | 40   |
| Period Length                                      | 76 mm  |
| Pole Length  | 3.04 m   |
| Pole Gap   | 24–200 mm  |
| Deflection Parameter                               | 5.4 (Max. Horizontal)<br>3.6 (Max. Vertical)<br>3.0 (Max. Helical) |

| <b>Bending Magnets</b> |              |
|------------------------|--------------|
| Type                   | Combined × 8 |
| Magnetic Length        | 1.728 m      |
| Bending Radius         | 2.2 m        |
| Bending Angle          | 45 deg.      |
| Pole Gap               | 55.2 mm      |
| Pole Width             | 140 mm       |
| Critical Energy        | 425 eV       |

(Last updated, August, 2024)

## Beamlines in 2023

Fumihiko Matsui

*UVSOR Synchrotron Facility, Institute for Molecular Science, Okazaki 444-8585, Japan*

UVSOR is one of the highest-brilliance light sources in the extreme-ultraviolet region among the synchrotron radiation facilities with electron energies of less than 1 GeV. The low natural emittance of the UVSOR-III storage ring, 17.5 nm-rad, was accomplished after the successful completion of the storage ring upgrade project (the UVSOR-III project) in 2012. Eight bending magnets and six insertion devices are available as synchrotron light sources at UVSOR. There are a total of thirteen operational beamlines. Eleven of them are the so-called “Public beamlines”, which are open to scientists from universities and research institutes belonging to the government, public organizations, private enterprises and also those from foreign countries. The beamline BL6U is the “In-house beamlines”, and are dedicated to the use of research groups within Institute for Molecular Science (IMS). The beamline BL1U is a partially “Public” and partially “In-house” beamline. There is one tender X-ray (TX) station equipped with a double-crystal monochromator, six extreme ultraviolet (EUV) and soft X-ray (SX) stations with grazing incidence monochromators, three vacuum ultraviolet (VUV) stations with normal incidence monochromators, two infrared (IR) stations equipped with Fourier Transform interferometers, and one direct radiation station located after two tandem undulators, as shown in the appended table (next page) for all available beamlines at UVSOR in 2023. The details of the updates for undulator beamlines are the followings.

- In **BL1U**, the development of a new light source and the utilization of gamma-rays are being carried out. This beamline is equipped with a tandem undulators with a buncher section, which can be used for free electron laser in the range from visible to deep UV, VUV coherent harmonic generation, and generation of spatiotemporal structured light such as an optical vortex beam, a vector beam and double-pulsed wave packets. It is also equipped with a femto-second laser system synchronized with the accelerator, which is used for the generation of Compton scattered gamma-rays. Users are provided with gamma-ray induced positron annihilation spectroscopy that can analyze nanometer-order defects in bulk materials. To increase the counting rate of annihilation gamma rays, an array detector with eight BaF<sub>2</sub> scintillators was developed. The measurement can be completed in a few hours for metal samples.
- In **BL3U**, the ultrathin-liquid cell for low-energy XAS has been developed. The studies of local structures of several aqueous solutions and various chemical processes in solution such as catalytic and electrochemical reactions, and laminar flows in microfluidics by using operando XAS in C, N, and O K-edges were demonstrated. Moreover, an argon gas window that is effective from 60 to 240 eV with the removal of high-order X-rays, which will develop chemical research since it includes K-edges of Li and B and L-edges of Si, P, S, and Cl was established.
- Resonant soft X-ray scattering (RSoXS) for soft materials is also applicable. RSoXS is similar to small angle X-ray scattering (SAXS) and can provide information on the mesoscopic structure (1-100 nm) of sample. This method has selectivity of elements, functional groups and molecular orientation. Since soft X-ray region include K-edge energies of light element (C, N, O), RSoXS is a powerful tool to investigate soft matters.
- **BL4U**, which is equipped with a scanning transmission soft X-ray microscope (STXM), is actively used not only by academic users but also by many industrial users. The STXM can be applied to wide range of sciences, such as polymer science, material science, cell biology, environmental science, and so on. In FY2020, it became possible to image the lithium K-edge with a spatial resolution of 72 nm. Final adjustments for the airtight sample transport system and the sample transport container were carried out for the organic substance analysis of the Hayabusa2 returned samples for the summer of FY2021.
- In **BL5U**, high energy resolution angle-resolved photoemission spectroscopy (ARPES) is available. Users can now use so-called “deflector mapping” for all kinetic energies and lens modes by using the latest version of ARPES analyzer. Users can also obtain spatial-dependence of the electronic structure of solid surfaces using micro-focused beam (50 μm). An alkali-metal deposition system has been installed. Potassium for example can be deposited while the sample is still mounted on the manipulator at low temperatures. As part of the development of spin-resolved ARPES, two-dimensional images of the spin-resolved spectrum of the Rashba splitting of Au(111) surface has been successfully obtained.
- At **BL6U**, one of the In-house beamlines, photoelectron momentum microscope (PMM), which is a new-concept multi-modal electronic structure analysis system with high resolution in real space and momentum space, has been installed and is in operation. A key feature of the PMM is that it can very effectively reduce radiation-induced damage by directly projecting a single

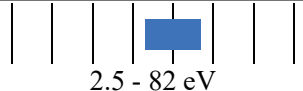
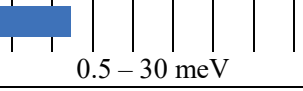
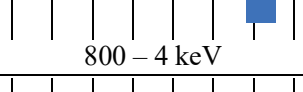
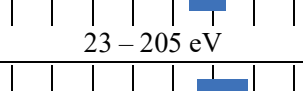
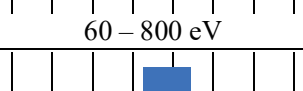
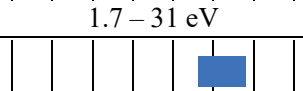
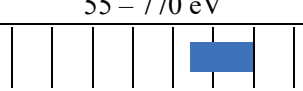

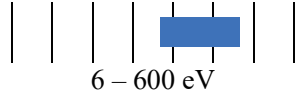
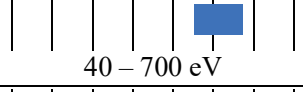
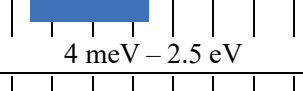
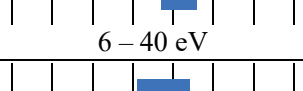
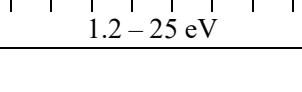

photoelectron constant energy contour in reciprocal space with a radius of a few  $\text{\AA}^{-1}$  or real space with a radius of a few hundred  $\mu\text{m}$  onto a 2D detector. Experiments such as valence band photoelectron spectroscopy on the micrometer scale and resonance photoelectron diffraction by soft X-ray excitation are performed. In FY2023, PMM's capabilities were further expanded by introducing an additional 2D spin filter. Two-dimensional images of the spin-resolved spectrum of the Rashba splitting of Au(111) surface has been also successfully obtained too following BL5U. In addition to grazing-incidence soft X-ray excitation, normal-incidence vacuum ultraviolet (VUV) beam with variable polarizations (horizontal/vertical) became also available at the same focal position of the PMM via a newly added branch from the next BL7U. This highly symmetrical measurement geometry completely eliminates the p-polarized linear dichroism effect in the circular dichroism measurements of valence band, making transition matrix element analysis

much simpler and reliable.

- At **BL7U**, high-energy resolution ARPES is available with extremely low energy of photons (6 eV~) using the low-temperature 6-axis manipulator with a sample temperature 4.5-350 K. In FY2021, the deflector-type detector for the hemispherical analyzer was installed to realize an effective 2D measurement with the automated manipulator control. Users can perform the measurement of the bulk sensitive electronic structure of solids and the high-throughput measurement for molecular materials using high-photoionization cross-section using low-excitation photon energy.

Those wishing to use the open and in-house beamlines are recommended to contact the appropriate beamline contact persons (see next page). Applications can be submitted at NOUS (<https://nous.nins.jp/user/signin>). All users are required to refer to the beamline manuals and the UVSOR guidebook, on the occasion of conducting the actual experimental procedures. For updated information on UVSOR, please see <http://www.uvsor.ims.ac.jp>.

## Beamlines at UVSOR

| Beamline | Monochromator / Spectrometer                                    | Energy Range   | Targets                | Techniques  | Contact                         |
|----------|---|--|------------------------|---|---------------------------------|
| BL1U     | Light Source Development<br>Gamma-ray<br>FEL                    |  2.5 - 82 eV      |                        | Irradiation (UV<br>and Gamma-rays)                    | Y. Taira<br>yostaira@ims.ac.jp  |
| BL1B     | Martin-Puplett FT-FIR   |  0.5 - 30 meV     | Solid                  | Reflection<br>Absorption                              | K. Tanaka<br>k-tanaka@ims.ac.jp |
| BL2A     | Double crystal  |  800 - 4 keV      | Solid                  | Reflection<br>Absorption                              | F. Matsui<br>matui@ims.ac.jp    |
| BL2B     | 18-m spherical grating<br>(Dragon)                              |  23 - 205 eV      | Solid                  | Photoemission   | S. Kera<br>kera@ims.ac.jp       |
| BL3U     | Varied-line-spacing<br>plane grating<br>(Monk-Gillieson)        |  60 - 800 eV      | Gas<br>Liquid<br>Solid | Absorption<br>Photoemission<br>Photon-emission        | H. Iwayama<br>iwayama@ims.ac.jp |
| BL3B     | 2.5-m off-plane Eagle   |  1.7 - 31 eV     | Solid                  | Reflection<br>Absorption<br>Photon-emission           | F. Matsui<br>matui@ims.ac.jp    |
| BL4U     | Varied-line-spacing<br>plane grating<br>(Monk-Gillieson)        |  55 - 770 eV    | Gas<br>Liquid<br>Solid | Absorption<br>(Microscopy)                            | T. Araki<br>araki@ims.ac.jp     |
| BL4B     | Varied-line-spacing<br>plane grating<br>(Monk-Gillieson)        |  25 eV - 1 keV  | Gas<br>Solid           | Photoionization<br>Photodissociation<br>Photoemission | H. Iwayama<br>iwayama@ims.ac.jp |
| BL5U     | Varied-line-spacing<br>plane grating<br>(Monk-Gillieson)        |  20 - 220 eV    | Solid                  | Photoemission   | K. Tanaka<br>k-tanaka@ims.ac.jp |
| BL5B     | Plane grating   |  6 - 600 eV     | Solid                  | Calibration<br>Absorption                             | K. Tanaka<br>k-tanaka@ims.ac.jp |
| BL6U*    | Variable-included-angle<br>varied-line-spacing<br>plane grating |  40 - 700 eV    | Solid                  | Photoelectron<br>Momentum<br>Microscopy               | F. Matsui<br>matui@ims.ac.jp    |
| BL6B     | Michelson FT-IR   |  4 meV - 2.5 eV | Solid                  | Reflection<br>Absorption<br>IR microscope             | K. Tanaka<br>k-tanaka@ims.ac.jp |
| BL7U     | 10-m normal incidence<br>(modified Wadsworth)                   |  6 - 40 eV      | Solid                  | Photoemission   | K. Tanaka<br>k-tanaka@ims.ac.jp |
| BL7B     | 3-m normal incidence  |  1.2 - 25 eV    | Solid                  | Reflection<br>Absorption<br>Photon-emission           | F. Matsui<br>matui@ims.ac.jp    |

**Yellow columns represent undulator beamlines.**

**\*In-house beamline**



# BL1U

## Light Source Development Station

### ▼ Description

BL1U is dedicated for developments and applications of novel light sources. This beamline is equipped with a dedicated tandem undulator for variable polarization with a buncher section, which can be used for free electron laser in the range from visible to deep UV, VUV coherent harmonic generation (CHG), and generation of spatiotemporal structured light such as an optical vortex beam, a vector beam and double-pulse wave packets. It is also equipped with a femto-second laser system synchronized with the accelerator, which is used for the generation of CHG, laser Compton scattered gamma-rays, and coherent THz radiation. Nowadays, material analysis by positron annihilation spectroscopy using laser Compton scattered gamma rays is actively used.

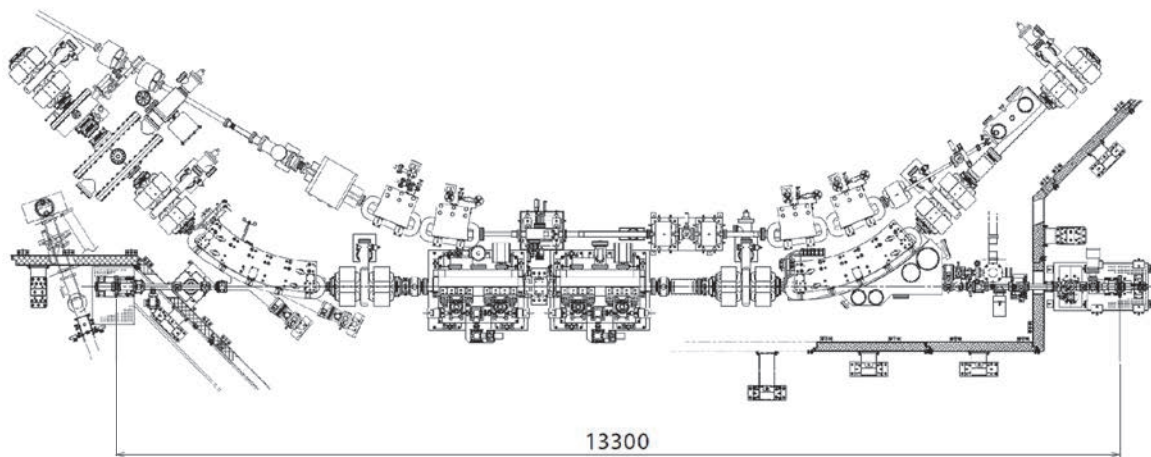


Fig. 1. Configuration of the free electron laser

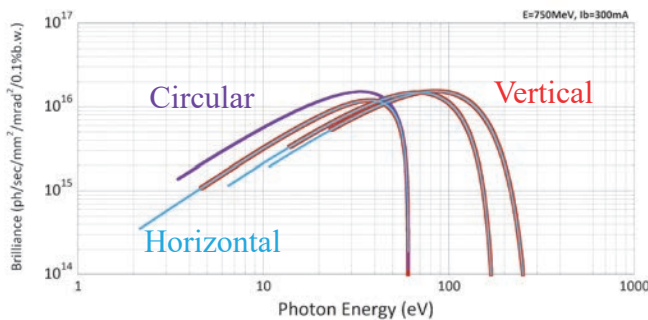


Fig. 2. Brilliance of BL1U Apple-II Undulator.

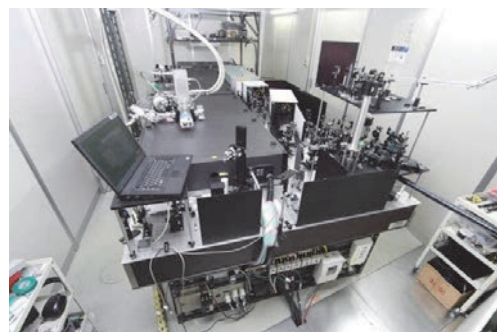


Fig. 3. Accelerator Synchronized Laser System.

### ▼ Technical Data of FEL

|                     |                 |
|---------------------|-----------------|
| Wave Length         | 199-800 nm      |
| Spectral Band Width | $\sim 10^{-4}$  |
| Polarization        | Circular/Linear |
| Pulse Rate          | 11.26 MHz       |
| Max. Ave. Power     | $\sim 1$ W      |

### ▼ Technical Data of Ti:Sa Laser

|                 |                          |
|-----------------|--------------------------|
| Wave Length     | 800 nm                   |
| Pulse Length    | 130 fsec                 |
| Oscillator      | 90.1 MHz                 |
| Pulse Energy    | 2.5 mJ    10 mJ    50 mJ |
| Repetition Rate | 1 kHz    1 kHz    10 Hz  |

# BL1B

## Terahertz Spectroscopy Using Coherent Synchrotron Radiation

### ▼ Description

Coherent synchrotron radiation (CSR) is a powerful light source in the terahertz (THz) region. This beamline has been constructed for basic studies on the properties of THz-CSR. However, it can be also used for measurements of reflectivity and transmission spectra of solids using conventional synchrotron radiation.

The emitted THz light is collected by a three-dimensional magic mirror (3D-MM, M0) of the same type as those already successfully installed at BL43IR in SPring-8 and BL6B in UVSOR-II. The 3D-MM was installed in bending-magnet chamber #1 and is controlled by a 5-axis pulse motor stage ( $x, z$  translation;  $\theta_x, \theta_y, \theta_z$  rotation). The acceptance angle was set at 17.5-34 degrees (total 288 mrad) in the horizontal direction. The vertical angle was set at  $\pm 40$  mrad to collect the widely expanded THz-CSR.

The beamline is equipped with a Martin-Puplett type interferometer (JASCO FARIS-1) to cover the THz spectral region from 4 to 240  $\text{cm}^{-1}$  ( $h\nu = 500 \mu\text{eV}$ -30 meV). There is a reflection/absorption spectroscopy (RAS) end-station for large samples ( $\sim$  several mm). At the RAS end-station, a liquid-helium-flow type cryostat with a minimum temperature of 4 K is installed.

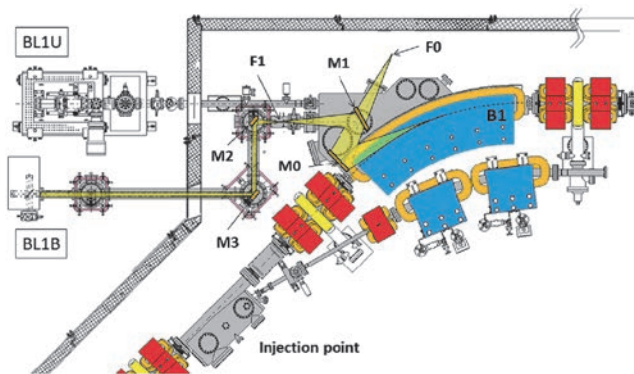


Fig. 1. Schematic top view of the beam extraction part of the THz-CSR beamline, BL1B. The three-dimensional magic mirror (3D-MM, M0) and a plane mirror (M1) are located in the bending-magnet chamber. A parabolic mirror (M2) is installed to form a parallel beam. The straight section (BL1U) is used for coherent harmonic generation (CHG) in the VUV region.

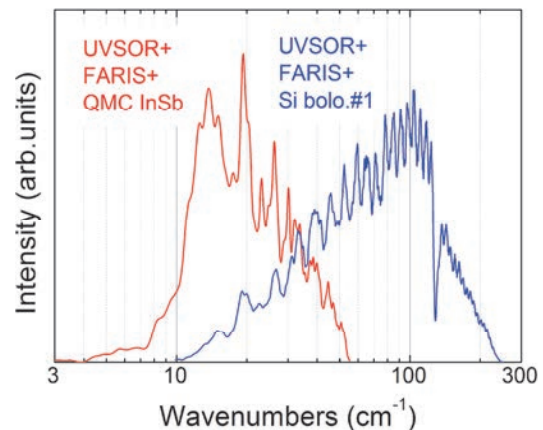


Fig. 2. Obtained intensity spectra with the combination of a light source (UVSOR), interferometer (FARIS-1), and detectors (Si bolometer and InSb hot-electron bolometer).

### ▼ Technical Data

|                                    |   |
|------------------------------------|---|
| Interferometer                     | Martin-Puplett (JASCO FARIS-1)                            |
| Wavenumber range<br>(Energy range) | 4-240 $\text{cm}^{-1}$<br>(500 $\mu\text{eV}$ -30 meV)    |
| Resolution in $\text{cm}^{-1}$     | 0.25 $\text{cm}^{-1}$                                     |
| Experiments                        | Reflection/transmission spectroscopy                      |
| Miscellaneous                      | Users can use their experimental system in this beamline. |

# BL2A

## Soft X-Ray Beamline for Photoabsorption Spectroscopy

### ▼ Description

BL2A is a soft X-ray beamline for photoabsorption spectroscopy. The beamline is equipped with a pre-focusing mirror and a double-crystal monochromator [1]. The monochromator serves soft X-rays in the energy region from 585 to 4000 eV using several types of single crystals, such as beryl, KTP (KTiOPO<sub>4</sub>), and InSb. The throughput spectra measured using a Si photodiode (AXUV-100, IRD Inc.) are shown in Fig. 1. The typical energy resolution ( $E/\Delta E$ ) of the monochromator is approximately 1500 for beryl and InSb.

There is a small vacuum chamber equipped with an electron multiplier (EM) detector. Photoabsorption spectra for powdery samples are usually measured in total electron yield mode, with the use of the EM detector. In addition, a hemispherical electron analyzer for photoelectron spectroscopy is equipped.

Recently, a new omnidirectional photoelectron acceptance lens (OPAL) has been developed aiming to realize  $2\pi$ -steradian photoelectron spectroscopy and photoelectron holography [2]. By combining OPAL and the existing hemispherical electron analyzer, a photoelectron spectrometer with high energy resolution can be realized, and a full range ( $\pm 90^\circ$ ) 1D angular distribution can be measured at once. This upgrade is currently in the commissioning phase.

[1] Hiraya *et al.*, Rev. Sci. Instrum. **63** (1992) 1264.

[2] H. Matsuda and F. Matsui, Jpn. J. Appl. Phys. **59** (2020) 046503.

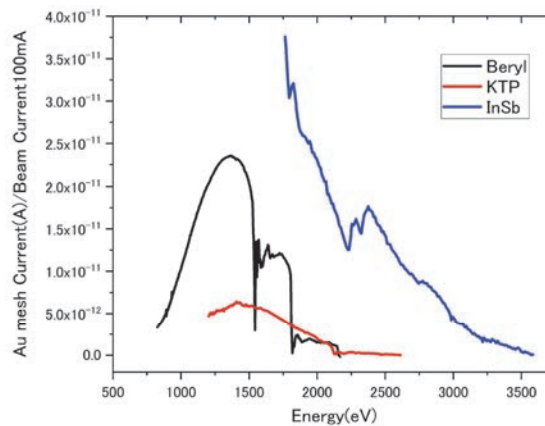


Fig. 1. Throughput spectra of the double-crystal monochromator at BL2A.

### ▼ Technical Data

|   |   |
|---|---|
| Monochromator                                       | Double crystal monochromator  |
| Monochromator crystals:<br>(2d value, energy range) | beryl (15.965 Å, 826–2271 eV), KTP (10.95 Å, 1205–3310 eV),<br>InSb (7.481 Å, 1764–4000 eV), Ge (6.532 Å, 2094–4000 eV) |
| Resolution  | $E/\Delta E = 1500$ for beryl and InSb  |
| Experiments   | Photoabsorption spectroscopy (total electron yield using EM and partial fluorescence yield using SDD)                   |

# BL2B

## *Photoelectron spectroscopy of molecular solids*

### ▼ Description

This beamline previously dedicated for experiments in the field of gas phase photoionization and reaction dynamics. Then, the beamline has been reconstructed for photoelectron spectroscopy of molecular solids with a new end station, and experiments can be performed from May 2014. The monochromator is a spherical grating Dragon type with 18-m focal length. High throughput ( $1 \times 10^{10}$  photons  $s^{-1}$ ) and high resolution ( $E/\Delta E = 2000 - 8000$ ) are achieved simultaneously under the condition of the ring current of 100 mA [1]. The optical system consists of two pre-focusing mirrors, an entrance slit, three spherical gratings (G1 - G3), two folding mirrors, a movable exit slit, and a refocusing mirror [2]. The monochromator is designed to cover the energy range of 23–205 eV with the three gratings: G1 (2400 lines  $mm^{-1}$ ,  $R = 18$  m) at 80–205 eV; G2 (1200 lines  $mm^{-1}$ ,  $R = 18$  m) at 40–100 eV; G3 (2400 lines  $mm^{-1}$ ,  $R = 9.25$  m) at 23–50 eV. The percentage of the second-order light contamination at  $h\nu = 45.6$  eV is 23 % for G2 or 7 % for G3.

A UHV chamber is placed downstream of the refocusing mirror chamber and equipped silicon photodiode, sapphire plate Au mesh and filters for absolute photon flux measurement, monitor the photon-beam position, relative photon flux measurements and attenuate higher order light, respectively.

The new end station consists of a main chamber with a hemispherical analyzer (SCIENTA R3000) and a liquid-He-cooled cryostat (temperature range of 15–400 K) with 5-axis stage, a sample preparation chamber with a fast-entry load-lock chamber and a cleaning chamber with LEED, ion gun for sputtering and IR heating unit.

[1] M. Ono, H. Yoshida, H. Hattori and K. Mitsuke, Nucl. Instrum. Meth. Phys. Res. A **467-468** (2001) 577.

[2] H. Yoshida and K. Mitsuke, J. Synchrotron Radiation **5** (1998) 774.

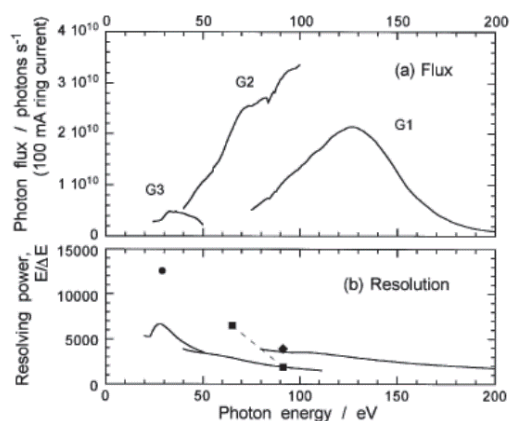


Fig. 1. Throughput from Dragon monochromator.

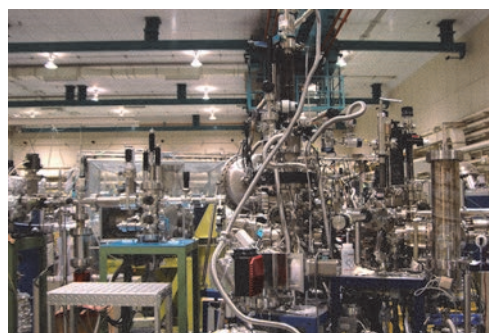


Fig. 2. End station of BL2B for photoelectron spectroscopy of molecular solids.

### ▼ Technical Data

|                  |   |
|------------------|---|
| Monochromator    | 18 m spherical grating Dragon-type                    |
| Wavelength Range | 23-205 eV   |
| Resolution       | 2000–8000 depending on the gratings                   |
| Experiments      | Angle-resolved ultraviolet photoelectron spectroscopy |



# BL3U

## Varied-Line-Spacing Plane Grating Monochromator for Molecular Soft X-Ray Spectroscopy

### ▼ Description

The beamline BL3U is equipped with an in-vacuum undulator composed of 50 periods of 3.8 cm period length. The emitted photons are monochromatized by the varied-line-spacing plane grating monochromator (VLS-PGM) designed for various spectroscopic investigations in the soft X-ray range. Three holographically ruled laminar profile plane gratings are designed to cover the photon energy range from 40 to 800 eV. The beamline has liquid cells for soft X-ray absorption spectroscopy (XAS) in transmission mode as shown in Fig. 1. The liquid cell is in the atmospheric helium condition, which is separated by a 100 nm thick  $\text{Si}_3\text{N}_4$  membrane with the window size of  $0.2 \times 0.2 \text{ mm}^2$  from the beamline in an ultrahigh vacuum condition. The thin liquid layer is assembled by using two 100 nm thick  $\text{Si}_3\text{N}_4$  membranes. The thickness of the liquid layer is controllable from 20 to 2000 nm by adjusting the helium pressures around the liquid cell in order to transmit soft X-rays. Liquid samples are exchangeable *in situ* by using a tubing pump. The liquid cell has two types of windows: one is the liquid part to obtain the soft X-ray transmission of liquid ( $I$ ), and the other is the blank part to obtain the transmission without liquid ( $I_0$ ). We can obtain the reliable XAS spectra based on the Lambert-Beer law  $\ln(I_0/I)$ . Since the liquid cell is in the atmospheric condition, we can measure XAS of liquid samples in the real environment. *Operando* XAS observation of several chemical reactions such as catalytic, electrochemical reactions are also possible by using our liquid cells developed for these purposes.

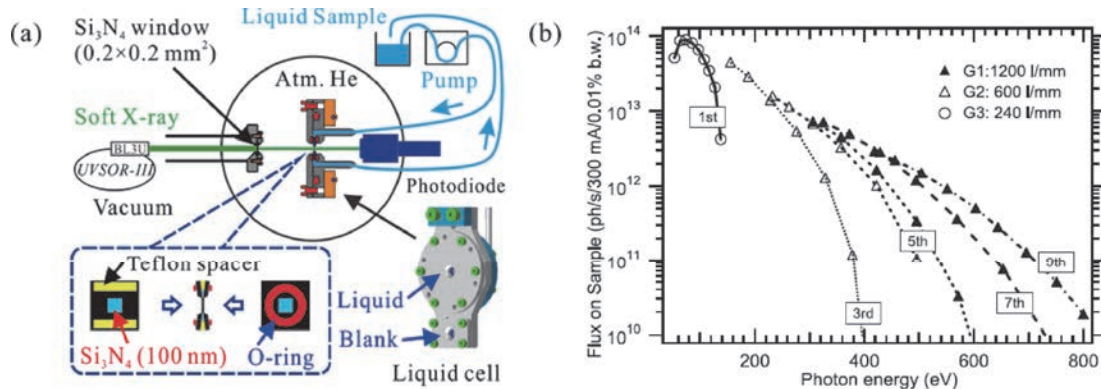


Fig. 1. (a) Schematics of a liquid cell for XAS in transmission mode settled in BL3U. The blowup shows a thin liquid layer assembled by two  $\text{Si}_3\text{N}_4$  membranes with the thickness of 100 nm. (b) Flux at the sample position with the resolving power of  $\lambda/\Delta\lambda=10^4$ .

### ▼ Technical Data

|               |   |
|---------------|---|
| Monochromator | Varied-line-spacing plane grating monochromator                   |
| Energy Range  | 40-800 eV   |
| Resolution    | $E / \Delta E > 10\,000$  |
| Experiments   | Soft X-ray absorption spectroscopy of liquid in transmission mode |

# BL3B (HOTRLU)

## VIS-VUV Photoluminescence and Reflection/Absorption Spectroscopy

### ▼ Description

BL3B has been constructed to study photoluminescence (PL) in the visible (VIS) to vacuum ultraviolet (VUV) region. This beamline consists of a 2.5 m off-plane Eagle type normal-incidence monochromator, which covers the VUV, UV, and VIS regions, i.e., the energy (wavelength) region of 1.7-31 eV (40-730 nm), with three spherical gratings having constant grooving densities of 1200, 600, and 300 l/mm optimized at the photon energies of  $\sim 20$ ,  $\sim 16$ , and  $\sim 6$  eV, respectively. The schematic side view and top view layouts are shown in Figs. 1(a) and 1(b), respectively. The FWHM of the beam spot at the sample position is 0.25 mm (V)  $\times$  0.75 mm (H). Low energy pass filters (LiF, quartz, WG32, OG53) can be inserted automatically to maintain the optical purity in the G3 (300 l/mm) grating region (1.7 $\sim$ 11.8 eV). Figure 2 shows the throughput spectra (photon numbers at a beam current of 300 mA) for each grating with entrance and exit slit openings of 0.1 mm (resolving power  $E / \Delta E$  of  $\sim 2000$  (G3,  $\sim 6.8$  eV)). Since both slits can be opened up to 0.5 mm, a monochromatized photon flux of  $10^{10}$  photons/s or higher is available for PL measurements in the whole energy region.

The end station is equipped with a liquid-helium-flow type cryostat for sample cooling and two detectors; one of which is a photomultiplier with sodium salicylate and the other a Si photodiode for reflection/absorption measurement. For the PL measurements in the wide energy region from VIS to VUV, two PL monochromators, comprising not only a conventional VIS monochromator but also a VUV monochromator with a CCD detector, are installed at the end station.

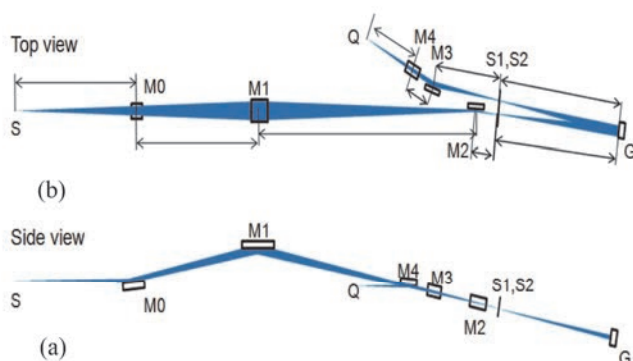


Fig. 1. Schematic layout of the BL3B (a) side view and (b) top view.

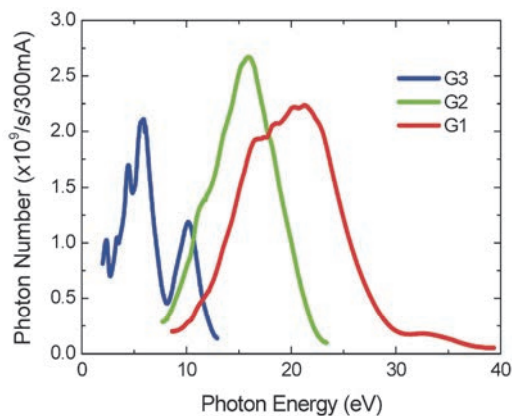


Fig. 2. Throughput spectra for each grating (G1:1200 l/mm, G2:600 l/mm and G3:300 l/mm) with  $S1 = S2 = 0.1$  mm.

### ▼ Technical Data

|                                     |   |
|-------------------------------------|---|
| Monochromator                       | 2.5 m normal-incidence monochromator  |
| Energy range                        | 1.7-31 eV (40~730 nm)   |
| Resolution ( $\Delta h\nu / h\nu$ ) | $\geq 12000$ (at $\sim 6.9$ eV, 0.02 mm slits, G1 (1200 l/mm))                |
| Experiments                         | Photoluminescence, reflection, and absorption spectroscopy, mainly for solids |

# BL4U

## Scanning Transmission X-ray Microscopy in the Soft X-ray Region

### ▼ Description

In the soft x-ray region, there are several absorption edges of light elements and transition metals. The near edge X-ray absorption fine structure (NEXAFS) brings detailed information about the chemical state of target elements. A scanning transmission X-ray microscope (STXM) in the soft X-ray region is a kind of extended technique of the NEXAFS with high spatial resolution. The STXM has a capability of several additional options, for example, in-situ observations, 3-dimensional observation by computed tomography and ptychography, by utilizing the characteristics of the X-rays. The STXM can be applied to several sciences, such as polymer science, material science, cell biology, environmental science, and so on.

This beamline equips an in-vacuum undulator, a varied-line-spacing plane grating monochromator and a fixed exit slit. The soft X-ray energy range from 50 to 770 eV with the resolving power ( $E/\Delta E$ ) of 6,000 is available. The aperture size of the fixed exit slit determines not only the resolving power but also the size of a microprobe. A Fresnel zone plate is used as a focusing optical device through an order select aperture and its focal spot size of ~30 nm is available at minimum. An image is acquired by detecting intensities of the transmitted X-rays by a photomultiplier tube with scintillator with scanning a sample 2-dimensionally. By changing the energy of the incident beam, each 2-dimensional NEXAFS image is stacked. A main chamber of STXM is separated from the beamline optics by a silicon nitride membrane of 50-nm thickness; therefore, sample folders can be handled in vacuum or in helium.

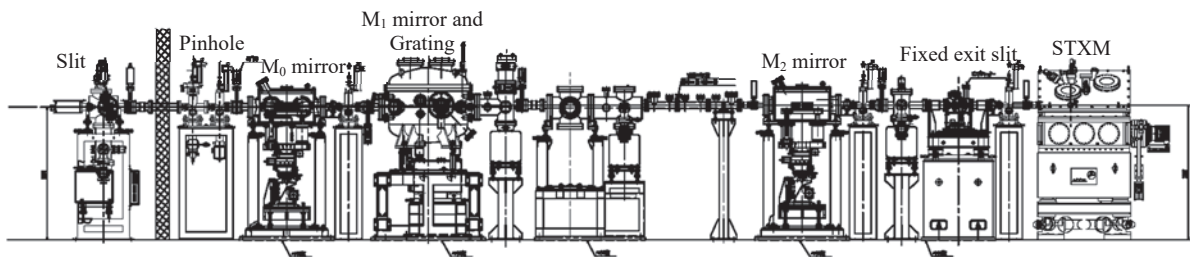


Fig. 1. Schematic image of BL4U

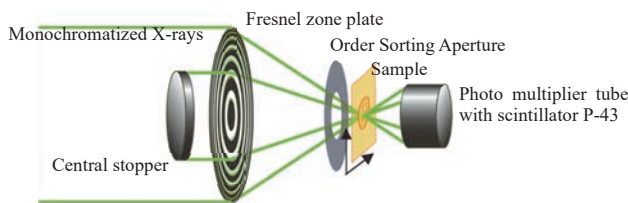


Fig. 2. Schematic image of STXM.

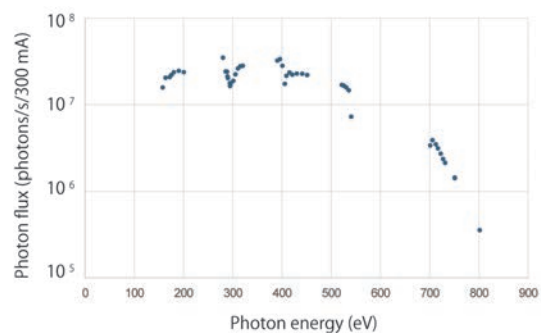


Fig. 3. Photon flux at the sample.

### ▼ Technical Data

|                                     |   |
|-------------------------------------|---|
| Energy range (E)                    | 50 -770 eV  |
| Resolving power (E/ΔE)              | ~6,000  |
| Photon flux on a sample (photons/s) | ~2×10 <sup>7</sup> @400 eV  |
| Focusing optical element            | Fresnel zone plate  |
| Spatial resolution                  | ~30 nm  |
| Experiments                         | 2-dimensional absorption spectroscopy   |
| Measurement environment             | standard sample folder in vacuum or in helium,<br>specially designed sample cell in ambient condition |

# BL4B

## Varied-Line-Spacing Plane Grating Monochromator for Molecular Soft X-Ray Spectroscopy

### ▼ Description

The beamline BL4B equipped with a varied-line-spacing plane grating monochromator (VLS-PGM) was constructed for various spectroscopic investigations in a gas phase and/or on solids in the soft X-ray range. Three holographically ruled laminar profile plane gratings with SiO<sub>2</sub> substrates are designed to cover the photon energy range from 25 to 800 eV. The gratings with groove densities of 100, 267, and 800 l/mm cover the spectral ranges of 25–100, 60–300, and 200–1000 eV, respectively, and are interchangeable without breaking the vacuum. Figure 1 shows the absolute photon flux for each grating measured using a Si photodiode (IRD Inc.), with the entrance- and exit-slit openings set at 50 and 50 μm, respectively. The maximum resolving power ( $E/\Delta E$ ) achieved for each grating exceeds 5000.

There is no fixed endstation on this beamline. A small vacuum chamber equipped with an electron multiplier (EM) detector is available. Soft X-ray absorption spectra of solid samples are usually measured by means of the total electron yield method using EM, and the partial fluorescence yield method using a silicon drift detector (SDD).

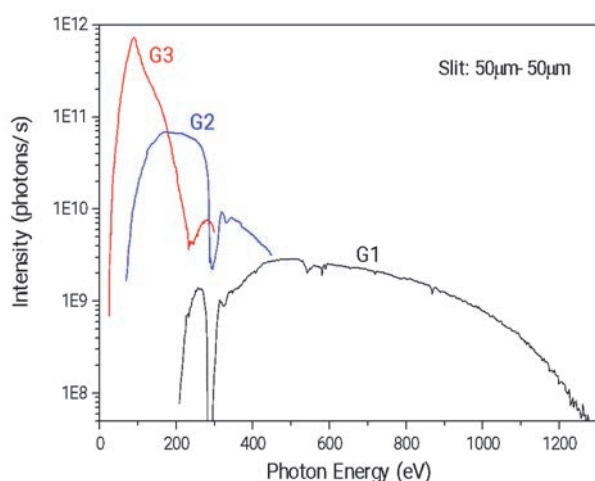


Fig. 1. Throughput from the VLS-PGM monochromator on BL4B.



Fig. 2. Photo of BL4B.

### ▼ Technical Data

|               |   |
|---------------|---|
| Monochromator | Varied-line-spacing Plane Grating Monochromator   |
| Energy range  | 25-1000 eV  |
| Resolution    | $E / \Delta E > 5000$ (at maximum)  |
| Experiments   | Soft X-ray spectroscopy (mainly, photoabsorption spectroscopy for solid targets by means of total electron yield method using EM and partial fluorescence yield method using SDD) |



# BL5U

## *Photoemission Spectroscopy of Solids and Surfaces*

### ▼ Description

Since the monochromator of BL5U was an old-style spherical grating type SGMTRAIN constructed in 1990s and the throughput intensity and energy resolution were poor, the whole beamline has been replaced to state-of-the-art monochromator and end station. The new beamline has been opened to users from FY2016 as high-energy resolution ARPES beamline. Samples can be cooled down to 3.8 K with newly developed 5-axis manipulator to perform high energy resolution measurements. Users can also obtain spatial-dependence of the electronic structure of solids using micro-focused beam ( $\sim 50 \mu\text{m}$ ). The new electron lens system makes it possible to obtain ARPES spectra without moving samples. This beamline will also have new capability to perform high-efficient spin-resolved ARPES in the future.

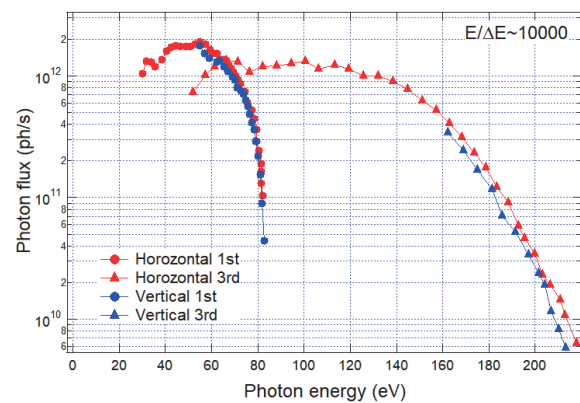
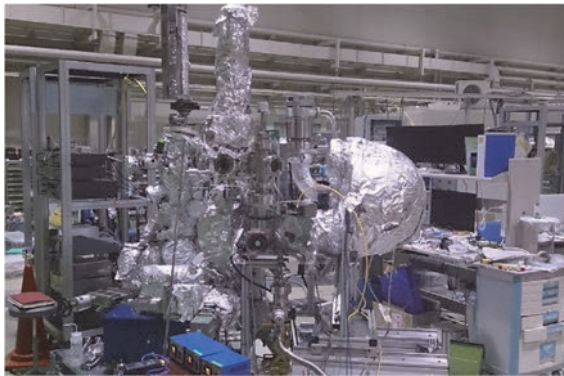


Fig. 1. Picture and photon flux of BL5U.

### ▼ Technical Data (Expected Performance)

|                  |  |
|------------------|--|
| Light source     | APPLE-II type undulator ( $\lambda_u = 60 \text{ mm}$ , $N = 38$ )<br>vertical/horizontal, right/left circular (depending on $h\nu$ )    |
| Monochromator    | Monk-Gillieson VLS-PGM   |
| Energy Range     | 20-200 eV  |
| Resolution       | $h\nu / \Delta E > 10,000$ for $< 10 \mu\text{m}$ slits  |
| Experiment       | ARPES, Space-resolved ARPES, Spin-resolved ARPES   |
| Flux             | $< 10^{12}$ photons/s for $< 10 \mu\text{m}$ slits (at the sample position)  |
| Beam spot size   | 23 (H) x 40 (V) $\mu\text{m}$  |
| Main Instruments | Hemispherical photoelectron analyzer with deflector scan (MBS A-1 Lens#4),<br>Liq-He flow cryostat with 5-axis manipulator (3.8 K-350 K) |

# BL5B

## Calibration Apparatus for Optical Elements and Detectors

### ▼ Description

BL5B has been constructed to perform calibration measurements for optical elements and detectors. This beamline is composed of a plane grating monochromator (PGM) and three endstations in tandem. The most upstream station is used for the calibration measurements of optical elements, the middle one for optical measurements for solids, and the last for photo-stimulated desorption experiments. The experimental chamber at the most downstream station is sometimes changed to a chamber for photoemission spectroscopy. The calibration chamber shown in Fig. 2 is equipped with a goniometer for the characterization of optical elements, which has six degrees of freedom, X-Y translation of a sample, and interchanging of samples and filters. These are driven by pulse motors in vacuum. Because the polarization of synchrotron radiation is essential for such measurements, the rotation axis can be made in either the horizontal or vertical direction (s- or p-polarization).

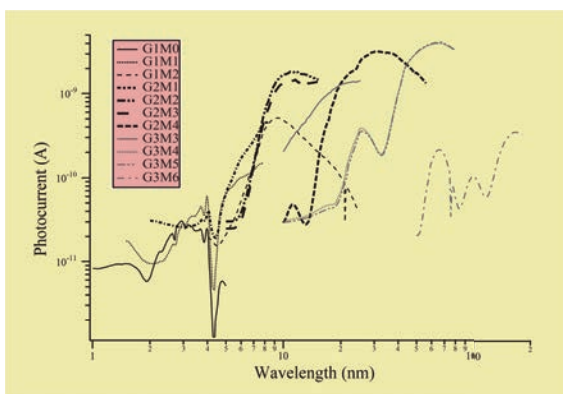


Fig. 1. Throughput spectra for possible combinations of gratings and mirrors at BL5B measured by a gold mesh.

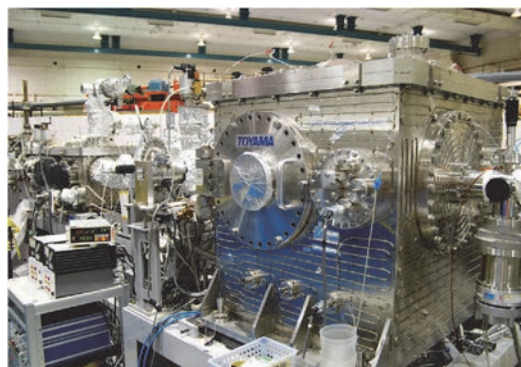


Fig. 2. A side view of the experimental chamber for calibration measurements.

### ▼ Technical Data

|               |   |
|---------------|---|
| Monochromator | Plane Grating Monochromator   |
| Energy range  | 6-600 eV (2-200 nm)   |
| Resolution    | $E / \Delta E \sim 500$   |
| Experiments   | Calibration of optical elements, reflection and absorption spectroscopy mainly for solids |

# BL6U

## Variable-Included-Angle / Variable-Line-Spacing Plane Grating Monochromator for Soft X-Ray photoelectron Spectroscopy

### ▼ Description

The beamline BL6U equipped with a variable-included-angle Monk-Gillieson mounting monochromator with a varied-line-spacing plane grating was constructed for various spectroscopic investigations requiring high-brilliance soft X-rays on solid surfaces. Through a combination of undulator radiation and sophisticated monochromator design (entrance slit-less configuration and variable-included-angle mechanism), using a single grating, the monochromator can cover the photon energy ranging from 40 to 500 eV, with resolving power of greater than 10000 and photon flux of more than  $10^{10}$  photons/s. Figure 1 shows an example of the monochromator throughput spectra measured using a Si photodiode, with the exit-slit opening set at 30  $\mu\text{m}$ , which corresponds to the theoretical resolving power of 10000 at 80 eV.

A new Momentum Microscope experimental station for photoelectron spectroscopy resolved in 3D momentum space with a microscopic field of view has been built at BL6U (SPECS KREIOS 150 MM). A momentum resolution of  $0.01 \text{ \AA}^{-1}$  in  $k_x/k_y$  as well as  $k_z$  is achieved. A spatial resolution of 50 nm, an energy resolution of 20 meV at 9 K, and a field of view of 2  $\mu\text{m}$  for ARPES are successfully demonstrated. This experimental station specializes in characterizing the electronic structure of surface atomic sites, thin films, molecular adsorbates, and bulk crystals. This method opens the door to direct observation of the Fermi surface of  $\mu\text{m}$ -sized crystals, which was difficult with conventional ARPES-type hemispherical analyzers.

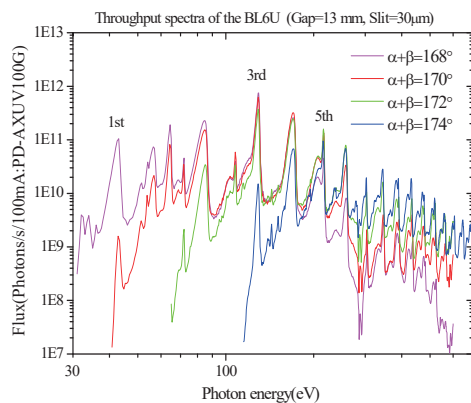


Fig. 1. Throughput spectra of the BL6U monochromator at various included angles.

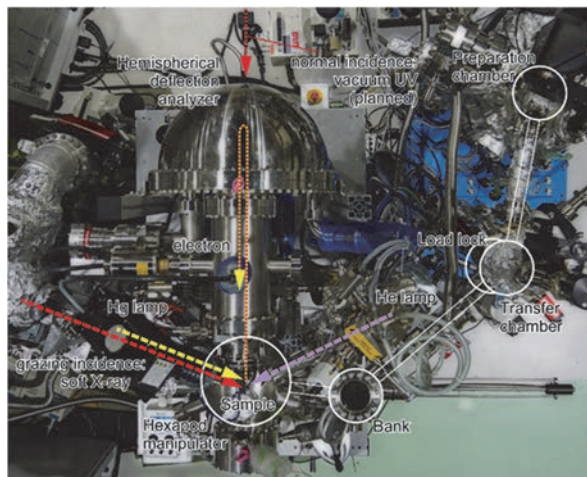


Fig. 2. Photograph of BL6U end station.

### ▼ Technical Data

|               |   |
|---------------|---|
| Monochromator | Variable-included-angle Varied-line-spacing Plane Grating Monochromator                 |
| Energy range  | 40-500 eV(practical)  |
| Resolution    | $E / \Delta E > 10000$ (at maximum)   |
| Experiments   | High-resolution soft X-ray spectroscopy (photoelectron spectroscopy for solid surfaces) |

# BL6B

## Infrared and Terahertz Spectroscopy of Solids

### ▼ Description

Synchrotron radiation (SR) has good performance (high brilliance and high flux) not only in the VUV and soft X-ray (SX) regions but also in the infrared (IR) and THz regions. BL6B covers the IR and THz regions. The previous beamline, BL6A1, which was constructed in 1985, was the pioneer in IRSR research. The beamline was deactivated at the end of FY2003 and a new IR/THz beamline, BL6B (IR), was constructed in FY2004. The front-end part including bending duct #6 was replaced with a new part having a higher acceptance angle ( $215 \text{ (H)} \times 80 \text{ (V)} \text{ mrad}^2$ ) using a magic mirror, as shown in Fig. 1.

There are two Michelson type interferometers in this endstation; with first one (Bruker Vertex70v), which covers a wide spectral region from  $30$  to  $20,000 \text{ cm}^{-1}$  ( $h\nu = 4 \text{ meV}-2.5 \text{ eV}$ ), reflection/absorption spectroscopy measurements of large samples (up to several mm) and IR/THz microscopy measurements of tiny samples (up to several tens of  $\mu\text{m}$ ) can be performed. For reflection/absorption spectroscopy measurements, a liquid-helium-flow type cryostat with a minimum temperature of  $4 \text{ K}$  is installed. The other interferometer (Jasco FT/IR-6100), which covers  $350$  to  $15,000 \text{ cm}^{-1}$  ( $h\nu = 45 \text{ meV}-1.8 \text{ eV}$ ), has been available for IR microscopy imaging measurements from FY2014. One can also perform ATR measurements using diamond ATR prism.

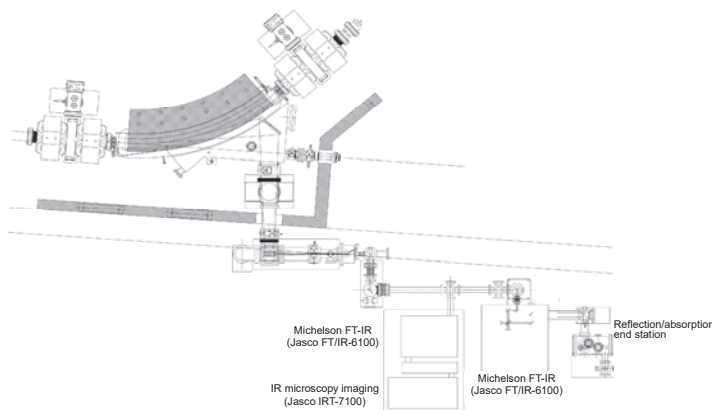


Fig. 1. Schematic top view of BL6B.

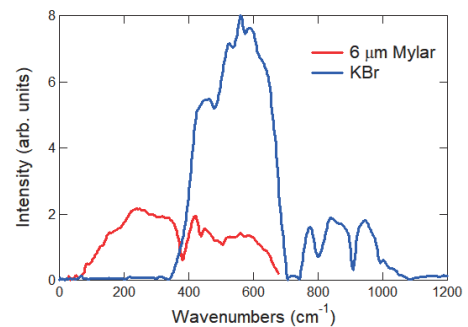


Fig. 2. Obtained intensity spectra with the combination of a light source (UVSOR), detector (Si bolometer), and interferometer (Bruker Vertex70v) with different beamsplitters ( $6 \mu\text{m}$  Mylar and KBr). (Only low energy side is shown).

### ▼ Technical Data

| Interferometer                  | Michelson (Bruker Vertex70v)  | Michelson (Jasco FT/IR-6100)  |
|---------------------------------|---|---|
| Wavenumber Range (Energy range) | $30-20,000 \text{ cm}^{-1}$<br>( $4 \text{ meV}-2.5 \text{ eV}$ )   | $350-15,000 \text{ cm}^{-1}$<br>( $45 \text{ meV}-1.8 \text{ eV}$ ) |
| Resolution in $\text{cm}^{-1}$  | $0.1 \text{ cm}^{-1}$   | $0.5 \text{ cm}^{-1}$   |
| Experiments                     | Reflectivity and transmission spectroscopy<br>THz Microspectroscopy | IR microscopy imaging (JASCO IRT-7000)<br>ATR spectroscopy          |



# BL7U (SAMRAI)

## Angle-Resolved Photoemission of Solids in the VUV Region

### ▼ Description

Beamline 7U, named the Symmetry- And Momentum-Resolved electronic structure Analysis Instrument (SAMRAI) for functional materials, was constructed to provide a photon flux with high energy resolution and high flux mainly for high-resolution angle-resolved photoemission spectroscopy, so-called “ARPES”, of solids [1]. An APPLE-II-type variable-polarization undulator is installed as the light source. The undulator can produce intense VUV light with horizontal/vertical linear and right/left circular polarization. The undulator light is monochromatized by a modified Wadsworth type monochromator with three gratings (10 m radius; 1200, 2400, and 3600 lines/mm optimized at  $h\nu = 10, 20,$  and  $33$  eV). The energy resolution of the light ( $h\nu/\Delta h\nu$ ) is more than  $10^4$  with a photon flux of  $10^{11}$ - $10^{12}$  ph/s or higher on samples in the entire energy region. The beamline has a photoemission end-station equipped with a 200 mm-radius hemispherical photoelectron analyzer (MB Scientific AB, A-1 analyzer) with a wide-angle electron lens and a liquid-helium-cooled cryostat with 6-axis pulse motor control. The main function of the beamline is to determine the electronic structure of solids and its temperature dependence in order to reveal the origin of their physical properties.

[1] S. Kimura, T. Ito, M. Sakai, E. Nakamura, N. Kondo, K. Hayashi, T. Horigome, M. Hosaka, M. Katoh, T. Goto, T. Ejima and K. Soda, *Rev. Sci. Instrum.* **81** (2010) 053104.

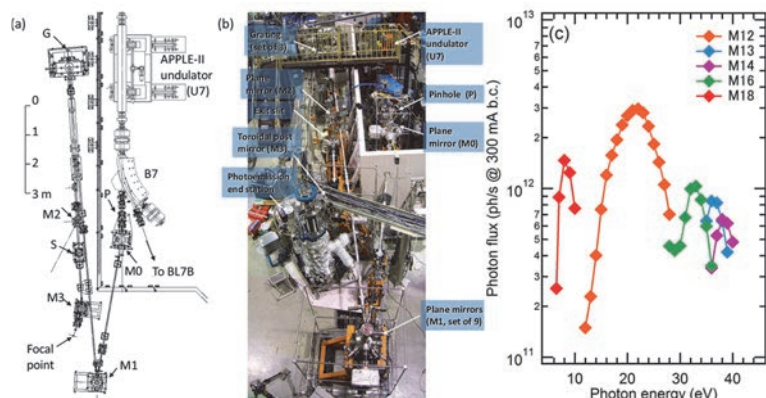


Fig. 1. SAMRAI beamline [(a), (b)] consisting of an APPLE-II type undulator (U7), a modified Wadsworth type monochromator (M0-S), and a high-resolution photoemission analyzer at the focal point. The monochromator has five major optical components: two plane mirrors (M0 and M1) with water cooling, one set of three spherical gratings (G), an exit slit (S), and one toroidal refocusing mirror (M3). (c) Example of flux intensity *versus* photon energy [1].

### ▼ Technical Data

|                                   |  |
|-----------------------------------|--|
| Light source                      | APPLE-II type undulator ( $\lambda_u = 76$ mm, $N = 36$ )<br>vertical/horizontal, right/left circular (depending on $h\nu$ ) |
| Monochromator                     | 10 m normal-incidence monochromator (modified Wadsworth type)  |
| Photon energy range               | 6 – 40 eV ( $\lambda = 30$ – 200 nm)   |
| Resolution ( $h\nu/\Delta h\nu$ ) | $E / \Delta E > 10000$ -50000  |
| Photon flux on sample             | $\geq 10^{11}$ - $10^{12}$ ph/s (depending on $h\nu$ )   |
| Beam size on sample               | 200 (H) $\times$ 50 (V) $\mu\text{m}^2$  |
| Experiments                       | Angle-resolved photoemission of solids<br>(MV Scientific A-1 analyzer, acceptance angle: $\pm 18$ deg)                       |

# BL7B

## 3 m Normal-Incidence Monochromator for Solid-State Spectroscopy

### ▼ Description

BL7B has been constructed to provide sufficiently high resolution for conventional solid-state spectroscopy, sufficient intensity for luminescence measurements, wide wavelength coverage for Kramers–Kronig analyses, and minimum deformation to the polarization characteristic of incident synchrotron radiation. This beamline consists of a 3-m normal incidence monochromator, which covers the vacuum ultraviolet, ultraviolet, visible, and infrared, i.e., the wavelength region of 50–1000 nm, with three gratings (1200, 600, and 300 l/mm). Two interchangeable refocusing mirrors provide two different focusing positions. For the mirror with the longer focal length, an LiF or a MgF<sub>2</sub> window valve can be installed between the end valve of the beamline and the focusing position. Figure 1 shows the absolute photon intensity for each grating with the entrance and exit slit openings of 0.5 mm. A silicon photodiode (AXUV-100, IRD Inc.) was utilized to measure the photon intensity and the absolute photon flux was estimated, taking the quantum efficiency of the photodiode into account.

The cooling system for the pre-focusing mirror has been removed, resulting in longer beam settling times. Currently, BL7B is opened during single bunch mode, but limited use is possible during multi bunch mode.

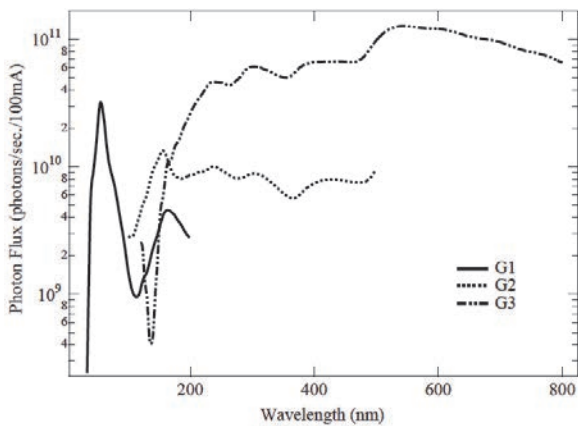


Fig. 1. Throughput spectra of BL7B measured using a silicon photodiode.

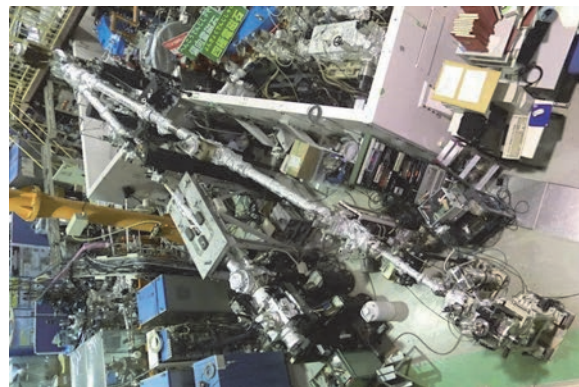


Fig. 2. Photo of BL7B.

### ▼ Technical Data

|                  |  |
|------------------|--|
| Monochromator    | 3 m Normal-Incidence Monochromator                                       |
| Wavelength Range | 50-1000 nm (1.2-25 eV)   |
| Resolution       | $E / \Delta E = 4000-8000$ for 0.01 mm slits                             |
| Experiments      | Absorption, reflection, and fluorescence spectroscopy, mainly for solids |



BL6U, 7U

## The Dual-Beamline Photoelectron Momentum Microscope at UVSOR

F. Matsui<sup>1,2</sup>, K. Hagiwara<sup>1</sup>, Y. Sato<sup>1</sup>, E. Nakamura<sup>1</sup>, T. Yano<sup>1</sup>, Y. Okano<sup>1</sup>, S. Makita<sup>1</sup>,  
R. Sagehashi<sup>1</sup>, S. Kera<sup>1,2</sup>, Shin-ichiro Tanaka<sup>3</sup> and S. Suga<sup>3</sup>

<sup>1</sup>UVSOR Synchrotron Facility, Institute for Molecular Science, Okazaki, Aichi, Japan

<sup>2</sup>The Graduate University for Advanced Studies (SOKENDAI), Okazaki, Aichi, Japan

<sup>3</sup>SANKEN, Osaka University, Ibaraki, Osaka, Japan

### 1. Introduction

Elucidating the behavior of electrons in materials is of great importance for the development of materials science and device engineering. Photoelectron spectroscopy (PES) provides deep insight into the nature of the atomic and electronic structure of solids. The demand for the development of PES technique has increased further in recent years. In particular, selective observation of electronic structures from micro-sized structures is desired by various scientific communities. Currently, research efforts on the  $\mu\text{m}$  and sub- $\mu\text{m}$  scale are underway around the world.

Photoelectron momentum microscopes (PMMs) are novel imaging photoelectron spectroscopy systems that combines a photoemission electron microscope (PEEM)-type objective lens with an energy filtering analyzer [1-3]. PMMs are revolutionizing the study of detailed electronic structures of materials and devices at the nm to tens of nm scale. We have constructed a PMM station [4,5] at BL6U [6]. This makes it possible to analyze the behavior of electrons on a  $\mu\text{m}$  scale. Furthermore, this advanced analytical and experimental station has been upgraded to enable the use of two undulator beamlines as excitation sources [7]. By branching off the existing vacuum ultraviolet (VUV) beamline BL7U, PMM can now simultaneously use tunable polarized VUV light in addition to the soft X-ray beam from beamline BL6U.

This world's first “*dual beamline photoelectron momentum microscope*” performs element-selective measurements using grazing incidence soft X-rays and

highly symmetric measurements using normal incidence VUV light at the same position on the sample and under the same conditions. Leveraging the flexibility of these light sources opens up new ways to analyze electron behavior in a multimodal manner. In particular, we emphasize that PES in normal incidence configuration is only available at this instrument at UVSOR worldwide. Such a highly symmetric configuration at normal incidence facilitates an accurate analysis of the valence orbitals, especially by photon polarization dependent transition matrix element analysis.

### 2. Details of dual beamline PMM station

#### 2.1 BL6U

Figure 1 shows the photograph of beamline BL6U, and BL7U together with newly constructed BL7U branch [7]. The schematic layout is shown in Fig. 2. In-vacuum undulator U6 installed as the light source for BL6U provides horizontal linearly-polarized soft X-ray ( $h\nu = 40\text{--}700\text{ eV}$ ) [8]. Figure 3(a) is a schematic of the beam and sample geometry. Typical width of the horizontal exit slit (H-slit) is set to 2–100  $\mu\text{m}$  in the vertical direction. The slit size of 25  $\mu\text{m}$  corresponds to the resolving power  $E/\Delta E$  of 10,000. A refocusing mirror of 1:1 convergence focuses the monochromatized soft X-ray onto the sample position. The incident X-ray beam is shaped by a vertical slit (V-slit) installed at the entrance of the analysis chamber so that the soft X-ray beam is maintained at the focal point of the analyzer. The final footprint of the irradiation spot

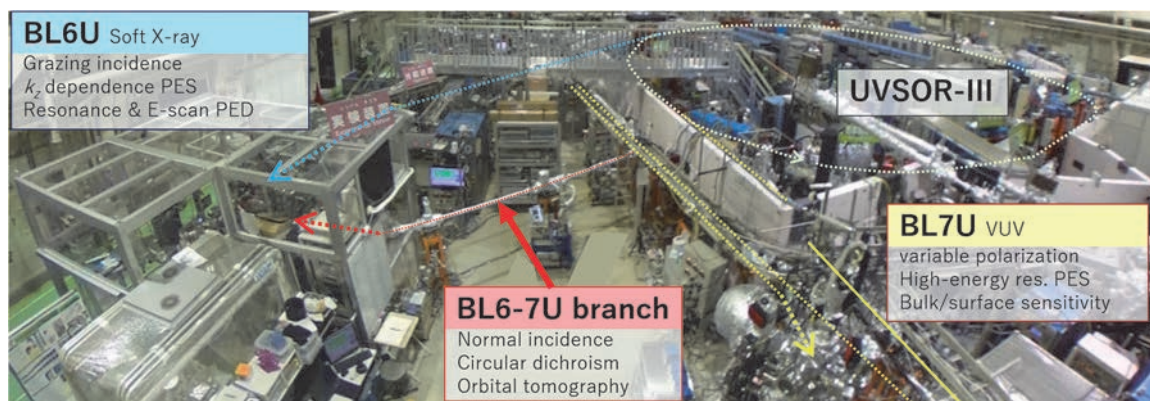


Fig. 1. Photograph of beamlines BL6U, BL7U and the newly constructed BL7U branch at the UVSOR Synchrotron Facility. The soft-X-ray (BL6U) and VUV (BL7U) beam-focusing optics and the PMM station are housed in a thermostatic hutch (300 K) so that the frame temperature fluctuation and beam fluctuation are suppressed within 0.1 K and 1  $\mu\text{m}$ , respectively, for hours.



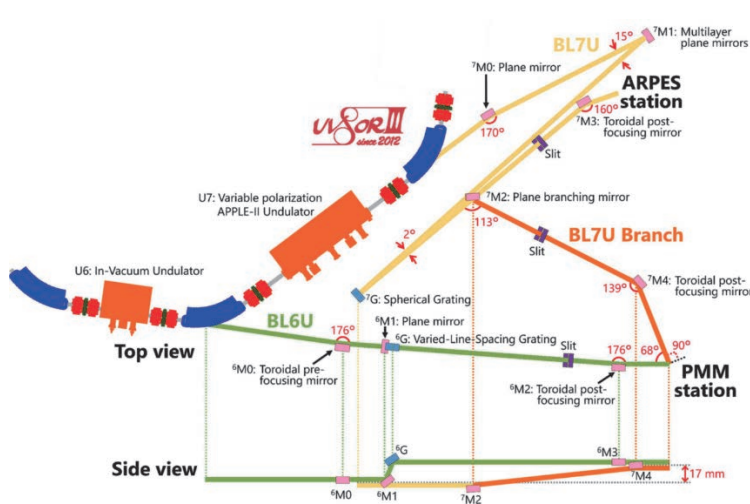


Fig. 2. Schematic layout of beamlines BL6U, BL7U and the newly constructed BL7U branch. Top and side views are shown. After the reflection on the <sup>6</sup>M1 mirror and the <sup>6</sup>G grating at BL6U, the beam path heightens by 17 mm. At BL7U, after reflection on the <sup>7</sup>M2 mirror, the beam is reflected upward and becomes 17 mm higher at the <sup>7</sup>M4 mirror than the undulator center. The beam focal point at the sample is accordingly higher than the height of the undulator center. From Ref. [6].

on the sample is 100–300  $\mu\text{m}$  horizontally and 2–100  $\mu\text{m}$  vertically. Typical maximum photon flux density is on the order of  $10^5$ – $10^7$  photons/s/ $\mu\text{m}^2$ . By varying the undulator gap from its optimal position, the photon flux density can be continuously reduced to achieve optimal measurement conditions for fragile molecular adsorbates and compound samples.

The sample surface lies in the  $xy$  plane. The upper direction of the vertical axis was defined as the  $+x$  direction. The photon beam from BL6U is incident at an angle of  $68^\circ$  from the sample surface normal ( $z$ ) axis. The PMM consists of a PEEM optics as an input lens [2] and a hemispherical deflection analyzer (HDA) [9]. The PEEM axis is set along the sample normal direction  $z$ . The  $yz$  plane, which contains the incident photon axis, its p-polarized electric field vector, and the PEEM optics axis, forms the mirror plane of the experimental geometry.

## 2.2 BL7U

Variable-polarization APPLE-II-type undulator U7 of BL7U can produce horizontal/vertical linearly and right/left circularly polarized VUV photons. The undulator light is guided to the <sup>7</sup>G spherical grating by the <sup>7</sup>M0 and <sup>7</sup>M1 plane mirrors and is monochromatized by the <sup>7</sup>G grating. High-energy-resolution ARPES experimental station (SAMRAI beamline) [10] is available at the end of BL7U.

The BL7U branch is designed to deliver a sufficiently high photon flux in both horizontal and vertical polarization to the same spot on the sample illuminated by the BL6U SX beam. By inserting/retracting the <sup>7</sup>M2 mirror installed after the <sup>7</sup>G grating, we can switch experiments of PMM at the end of BL7U branch [7] or ARPES at the end of BL7U [10]. The reflectance for the horizontally polarized light is lower than that for vertically polarized light and even becomes zero in the case of the Brewster angle. In order to avoid this configuration and also to hold a workspace for BL7U users, the beamline arrangement with a reflection angle of  $113^\circ$  at the <sup>7</sup>M2 mirror and  $139^\circ$  at the <sup>7</sup>M4 mirror was adopted. After reflection on the <sup>7</sup>M4 mirror, the

beam goes horizontally and the beam focal point of BL7U branch matches that of BL6U. The photon beam from BL7U comes in along the surface normal axis (s-polarized). The light linearly polarized in either  $xz$  or  $yz$  planes, *i.e.*, horizontally polarized light (H-pol.) and vertically polarized light (V-pol.), respectively, is available at the PMM experimental station. We are currently commissioning the undulator U7 for

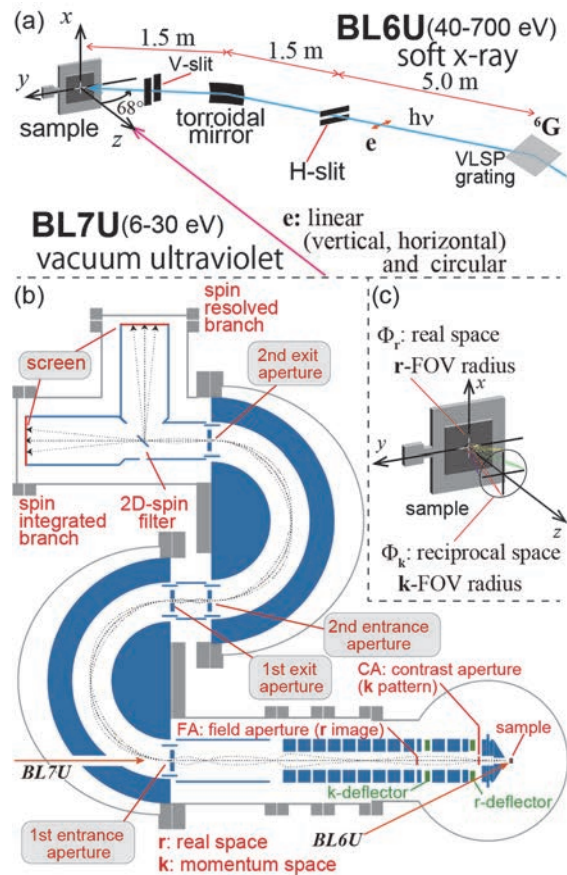


Fig. 3. (a) Incidence of photon and sample orientation. (b) Schematic drawing of photoelectron momentum microscope. (c) Fields of view (FOV) in real and reciprocal spaces.



generating circularly polarized VUV light.

Note that the use of the SAMRAI beamline and the branch PMM beamline is exclusive and cannot be used simultaneously. Fortunately, the position repeatability of  $^7\text{M}2$  makes it possible to switch between them in a short time. Currently, part of the beamtime at BL7U (about two weeks per semester) is allocated to developmental use at the branch.

### 2.3 PMM sample stage and chamber

The sample manipulator is equipped with a six-axis sample motion system (HESTIA) and a liquid-helium-flow cryostat. Samples can be cooled down below 10 K and heated up to 400 K. During the cooling process, the sample position shifted within 10  $\mu\text{m}$ . The soft-X-ray (BL6U) and VUV (BL7U) beam-focusing optics and the PMM station (SPECS KREIOS 150MM DI spin) is housed in a thermostatic hutch (300 K). Within the hutch, the frame temperature fluctuation and beam fluctuation are suppressed within 0.1 K and 1  $\mu\text{m}$ , respectively, for hours in our system.

Bellows with a diameter of 35 mm are used to connect the PMM analytical chamber to each of the two beamlines and to the preparation chamber complex. The vacuum force pulls the vacuum chamber horizontally from three directions, so if left alone, it will constantly be pulled toward BL7U. To prevent this, we used a 10-kg weight as a counterbalance to ensure that the chamber remained stable and in the same position.

### 2.4 PEEM column and HDA

The diffraction pattern is projected onto the back focal plane at the contrast aperture (CA) position (Fig.3(b)). The sample image is magnified 10 times in the first image plane at the FA position by the objective lens at an extraction voltage of 15 keV. By decreasing (increasing) the extraction voltage, the projection range in momentum space at the CA position is decreased (increased), while the size of real-space field of view (FOV) at the FA position is increased (decreased). The second half of the PEEM lens switches between microscopy (R mode) and momentum (K mode) observations (Fig.4). Further-more, the magnification of the sample image or reciprocal space pattern can be varied by setting multilens parameters. A real space image ( $x, y$ ) or reciprocal space pattern ( $k_x, k_y$ ) at the PEEM lens exit is transferred through the transfer lens and then projected onto the HDA entrance.

Apertures of different sizes can be selected for the HDA entrance and exit, as well as CA and FA, allowing control over the cropping extent of the 2D data projected onto them. When the CA and FA are fully open for electrons with sufficiently large kinetic energies and the extraction voltage is fixed, then the performance of the PMM is determined by the HDA apertures. The maximum r-FOV in the R mode ( $\Phi_r^R$ ) and the maximum k-FOV in the K mode ( $\Phi_k^K$ ), are determined by the magnification factor and the extraction voltage (Fig.3(c)). The k-FOV in the R mode ( $\Phi_k^R$ ) and the

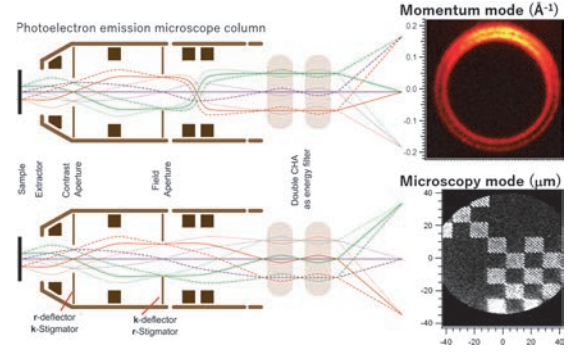


Fig. 4. Trajectory of electron in the PEEM column operated in momentum and microscopy modes. Field and contrast apertures are used to select the region of interests in real and reciprocal spaces in momentum and microscopy modes, respectively. The Rashba surface state of Au(111) surface and a checkerboard pattern are shown as examples for R and K mode observations.

r-FOV in the K mode ( $\Phi_r^K$ ) are proportional to the diameter of the HDA entrance aperture. See Ref. [11] for details. By choosing the appropriate aperture size for the CA and FA, we can control the k-FOV and r-FOV, respectively, and realize momentum-selective photoelectron microscopy and domain-selective momentum-resolved PES, respectively [4,12]. Note that when the photoelectron momentum,  $k_{\parallel, \text{max}} = 0.5123\sqrt{E_{\text{kin}}}k$ , is smaller than  $\Phi_k$ , photoelectrons emitted to all hemispheres are projected onto the screen.

PMMs utilize the imaging function of the HDA. Only electrons in the energy window centering on a specific energy that corresponds to the path energy ( $E_{\text{pass}}$ ) reach the HDA exit. At this exit aperture position, the real space image or reciprocal space pattern at the HDA entrance position is reconstructed. Recently, we upgraded the PMM with a single HDA [4,11] to the PMM with twin HDAs [7]. For the normal incidence experiment, the entrance slit of the first HDA is set to be open so that the beam can go through the optical lens of the PMM and arrive at the sample position. The exit slit of the first HDA is set to smaller one instead [13].

### 2.5 Detector

A Fourier transform lens converts this two-dimensional (2D) electron distribution from the real space to the reciprocal space, or vice versa, and projects it onto a fluorescent screen. This screen image is digitized by a CMOS camera. The volume data of band dispersion  $I(E, k_x, k_y)$  or micro-spectroscopy  $I(E, x, y)$  were constructed by measuring a series of 2D constant energy contours (CECs) of band ( $k_x$  versus  $k_y$ ) [12] and PEEM images ( $x$  versus  $y$ ) [5], respectively, as a function of the binding energy,  $E_{\text{binding}}$ .

An In(001) single crystal on a retractable manipulator is installed as a 2D spin filter. By retracting and inserting the spin filter, spin-integrated and spin-resolved photoelectron 2D intensity distribution data are acquired by one of two identical 2D detectors,

respectively (Fig. 3(b)).

### 3. Examples of comprehensive valence band characterization

#### 3.1 Advantage of 2D-CEC measurement

In the past, to measure a wide range of angular distributions using analyzers with small acceptance angles, the sample orientation was rotated in 2D ( $\theta$ ,  $\phi$ ) and the data was spliced together. This measurement style remains the standard and effective method for spin-polarized angle-resolved PES. The equivalent set of data may be now acquired by using a conventional HDA with the latest deflection-type lenses; measuring 2D  $I(E_{\text{binding}}, k_y)$  data as a function of  $k_x$  [8,14]. Furthermore, the use of the PMM is much more efficient than the use of such a method for measuring  $I(k_x, k_y)$ . The PMM that can simultaneously measure 2D CEC data eliminates the need to reorient the sample step-by-step, increasing the detection efficiency and reliability. Since the 2D Fermi surface can be simultaneously observed in real time [15] by our system, the use of the PMM is much better for confirming the location dependence of heterogeneous samples and polycrystalline samples, aligning the crystal orientation, and performing microscopic Fermi surface measurements within a good quality location [16]. Rotating the azimuthal angle of the sample can change the orientation of the electric field vector of incident photon (e) for evaluating the matrix element effect for atomic orbital analysis of valence band and molecular orbitals [17]. Short measurement times help to reduce possible damage of fragile molecular adsorbates and compound samples. Furthermore, 2D spin-polarized PMM measurements are a cutting-edge application of the CEC projection-type energy analyzer.

#### 3.2 Normal and grazing incidence photoemission

Figure 5 shows the 2D momentum ( $k_x, k_y$ ) distribution of photoelectron intensity of Au(111) at the Fermi level with an energy window of  $\pm 50$  meV [7]. The measurements were performed with V-pol. light at  $h\nu = 20$  eV (a, c) and H-pol. light at  $h\nu = 20$  eV from BL7U branch (b). Note that, in Figs. 5(a-c), we captured all photoelectrons emitted up to the emission angle of  $\theta = \pm 90^\circ$  (or within the emission cone of  $2\pi$  steradian) by the PMM, covering the maximum wide  $k_{\parallel}$  space. Furthermore, Figs.5(d) and (e) show the 2D patterns measured using p-polarized light at  $h\nu = 100$  eV and 80 eV, respectively, from BL6U. Shockley surface states centered at the  $\Gamma$  point as small circular contours is clearly observed with p-polarized excitation (Figs.5(d-e)). These features exhibit very weak intensity for normal incidence light (Figs.5(a-c)). This surface state mainly comprises  $6s$  and  $6p_z$  orbitals. In the normal-incidence geometry, the transition-matrix element from the initial  $s$  and  $p_z$  orbitals becomes 0 at the photoemission direction orthogonal to the excited electric field vector. The relationship between the orbital angular momentum and the effects of the transition matrix elements can be directly investigated

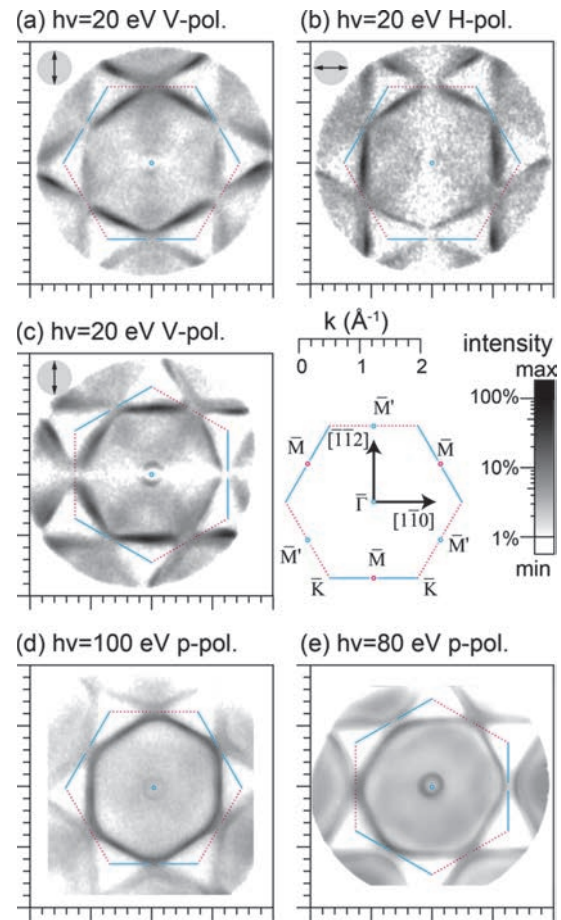


Fig. 5. 2D momentum ( $k_x, k_y$ ) distribution of the photoelectron intensity of the Au(111) surface at the Fermi level plotted on a logarithmic contrast scale. Measurements were performed with V-pol. at  $h\nu = 20$  eV (a, c), H-pol. at  $h\nu = 20$  eV from the BL7U branch (b) and p-pol. at  $h\nu = 100$  eV from BL6U (d). (e) High-resolution measurement taken using p-pol. at  $h\nu = 80$  eV from BL6U. In (c) and (e), the sample is in-plane rotated by  $-30^\circ$ . The upper left insets describe the experimental geometry of the electric field vector of the incident light. From Ref. [7].

using this normal incidence geometry.

#### 3.3 3D band dispersion and 3D Fermi surface

3D band dispersion data  $I(E_{\text{binding}}, k_x, k_y)$  can be obtained by scanning the kinetic energy ( $E_{\text{kin}}$ ) with a fixed excitation photon energy or by scanning the excitation photon energy with a fixed  $E_{\text{kin}}$ . The Fermi surface and valence band dispersion in a 3D momentum space are obtained by measuring the CECs at the Fermi level and at certain binding energies while sweeping the photon energy and kinetic energy of the photoelectron (constant initial state mode) [18].

#### 3.4 Soft X-ray resonance PES

Resonant photoelectron spectroscopy (RPES) is a widely used technique for highlighting specific elemental components of the valence band by adjusting the photon energy to a core-level excitation threshold.



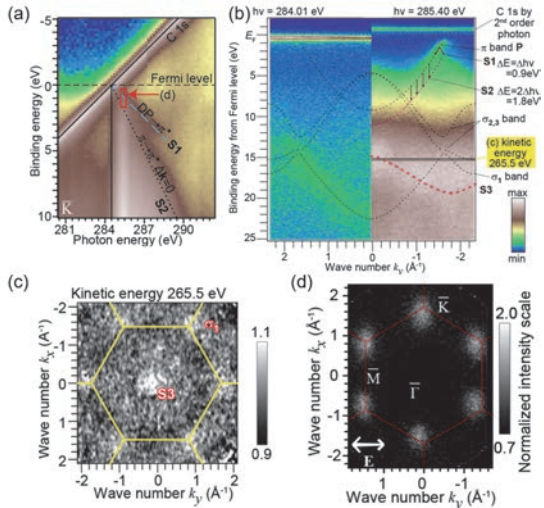


Fig. 6. (a) Momentum-resolved intensity maps at  $\bar{K}$  as functions of the binding energy and excitation photon energy near C K-shell absorption threshold. A logarithmic color scale was used for the contrast gradation. (b) Valence photoelectron and Auger electron spectra along the  $\bar{\Gamma}\bar{K}$  direction excited at the photon energy of 284.01 eV and 285.40 eV. Black (red) dotted lines indicate the valence band (Auger electron) dispersions. (c) Momentum-resolved Auger electron intensity distribution (c) at the photon and photoelectron kinetic energy of 285.40 eV and 266.5 eV, respectively, and (d) at the binding energy and photon energy ranges of 0.4–1.6 eV and 285.3–285.5 eV, respectively. A linear color scale was used for the normalized intensity contrast gradation. Six bright spots at  $\bar{K}$  points correspond to S1 shakeup process. After Ref. [19].

In RPES, the valence band dispersion around the excitation threshold of the core level is measured. We measured the momentum-resolved RPES of graphite

crystals and found unique dispersion structures embedded in Auger electrons (Fig. 6). This phenomenon was clarified based on the conservation and transfer of momentum [19,20]. This element-selective valence excitation technique provides a versatile means for creating and characterizing a valence exciton band selectively and is effective for investigation of various materials.

### 3.5 Dark Field imaging

The dark-field imaging technique has been developed for various electron and X-ray diffraction methods to select diffraction spots in the momentum space and visualize the spatial distribution of specific domains. We have applied this dark-field imaging technique to PMMs and established a momentum-selective photoelectron microscopy method, which is a quite useful for microscopic electronic structure investigations [12]. The  $\pi$ -dispersion of the valence band of graphite is the strongest at the M saddle point in the Brillouin zone (BZ). Selectively measuring the photoelectron intensity in the M direction of each region resulted in the successful projection of photoelectron microscopic images with each region highlighted with a resolution of approximately 100 nm. This momentum-selective photoelectron microscopy technique was also applied to visualize the single-atomic-height step edges on the graphite surface [18]. An image of graphite step edge along zig-zag atomic bonding direction (Fig. 7) was obtained by selecting one of the three-fold symmetric L-point photoelectron intensities characteristic of different terrace atomic arrangements.

### 4. Outlook

The most distinctive advantage of PMM is its snapshot-style of measuring photoelectron CEC in real

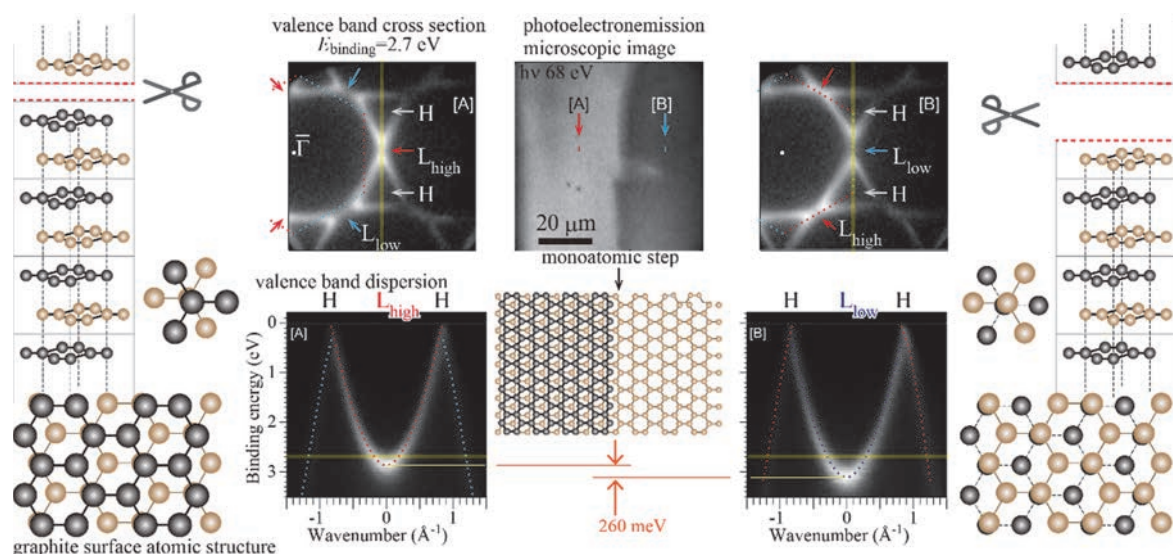


Fig. 7. Graphite surface microscopic image and valence band structure together with atomic structure models. The valence band cross-sections and dispersions of two different graphite terrace regions are shown. A step edge is visualized in  $\mu\text{m}$ -scale area image by selecting one of the three-fold symmetric L-point photoelectron intensities characteristic of different terrace atomic arrangements. After Ref. [18].

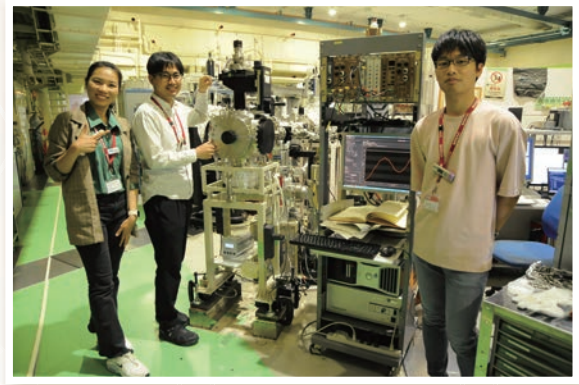
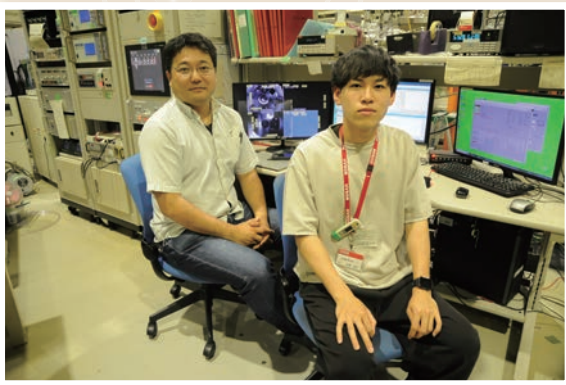
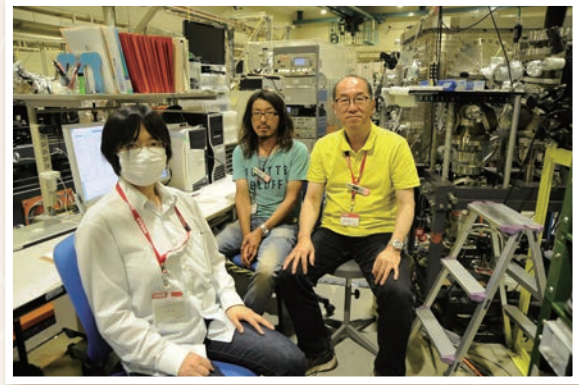
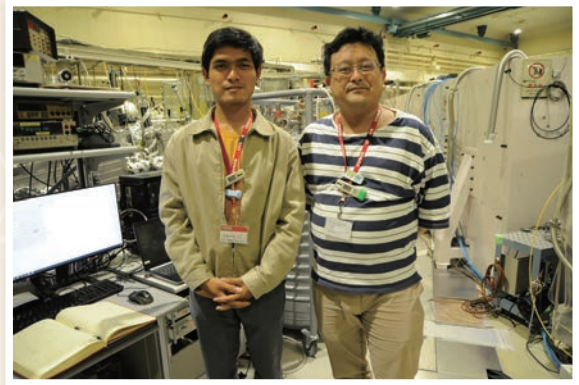
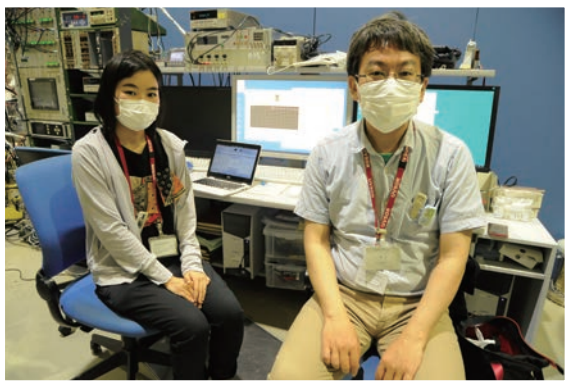
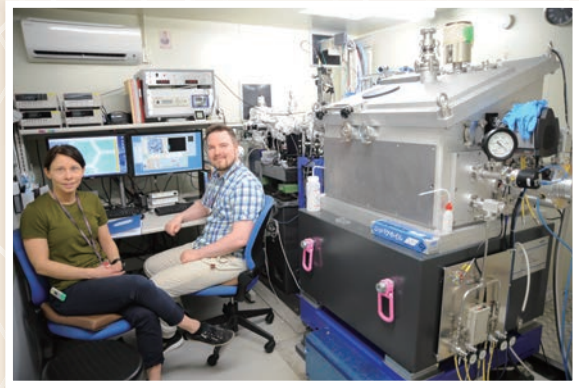
and reciprocal spaces. Recently we succeeded in the development of on-the-fly scans for temperature-dependent Fermi surface and valence band measurements during phase transitions, taking advantage of the rapid acquisition (seconds to minutes) of CECs. Polarization-dependent transition matrix elemental analysis is underway to study the molecular orbitals of fragile organic adsorbates on surfaces [20,21]. Finally, our main goal is to employ all these techniques with spin polarization sensitivity. We have just started obtaining spin-polarized valence band dispersion data for typical materials having spin polarized surface states. The combination of PMM with synchrotron SX and VUV undulators paves the way for comprehensive characterization of atomic orbitals and spins in the Fermi surface and valence band on the  $\mu\text{m}$  scale.

### References

- [1] B. Kromker, *et al.*, *Rev. Sci. Instrum.* **79**, 053702 (2008).
- [2] C. Tusche, *et al.*, *Ultramicroscopy* **159**, 520 (2015).
- [3] G. Schönhense, *et al.*, *Rev. Sci. Instrum.* **91**, 123110 (2020).
- [4] F. Matsui, *et al.*, *Jpn. J. Appl. Phys.* **59**, 067001 (2020).
- [5] S. Makita, *et al.*, *e-J. Surf. Sci. Nanotechnol.* **19**, 42 (2021).
- [6] H. Ota, *et al.*, *J. Phys.: Conf. Ser.*, **2380**, 012003 (2022).
- [7] K. Hagiwara, *et al.*, *J. Synchrotron Radiat.* **31**(3) 540-546 (2024).
- [8] H. Yamane, *et al.*, *Rev. Sci. Instrum.* **90**, 093102 (2019).
- [9] C. Tusche, *et al.*, *Ultramicroscopy* **206**, 112815 (2019).
- [10] S.-I. Kimura, *et al.*, *Rev. Sci. Instrum.* **81**, 053104 (2010).
- [11] F. Matsui, *et al.*, *Rev. Sci. Instrum.* **94**, 083701 (2023).
- [12] F. Matsui, *et al.*, *J. Phys. Soc. Jpn.* **91**, 094703 (2022).
- [13] C. Tusche, and J. Kirschner, (2006). German Patent DE102014019408.
- [14] Y. Ishida and S. Shin, *Rev. Sci. Instrum.* **89**, 043903 (2018).
- [15] T. Kato, *et al.*, *Phys. Rev. Lett.* **129**, 206402 (2022).
- [16] E. Hashimoto, *et al.*, *Jpn. J. Appl. Phys.* **61**, SD1015 (2022).
- [17] O. Endo, *et al.*, *J. Phys. Chem. C* **126**, 15971 (2022).
- [18] F. Matsui and S. Suga, *Phys. Rev. B* **105**, 235126 (2022).
- [19] F. Matsui, *et al.*, *J. Phys. Soc. Jpn.* **90**, 124710 (2021).
- [20] Y. Hasegawa, *et al.*, *e-J. Surf. Sci. Nanotechnol.* **20**, 174 (2022).
- [21] O Endo *et al.*, *e-J. Surf. Sci. Nanotechnol.* **21**, 236 (2023).



# *UVSOR User 1*





## *UVSOR User 2*

